Geochemistry, Geophysics, Geosystems

RESEARCH ARTICLE
10.1029/2019GC008573

Special Section:
Carbon degassing through volcanoes and active tectonic regions

Volcanic Gas Emissions Along the Colombian Arc Segment of the Northern Volcanic Zone (CAS-NVZ): Implications for volcano monitoring and volatile budget of the Andean Volcanic Belt

J. Lages[1], Z. Chacón[2], V. Burbano[3], L. Meza[4], S. Arellano[5], M. Liuzzo[6], G. Giudice[6], A. Aiuppa[1], M. Bitetto[1], and C. López[2]

[1]Dipartimento DiSTeM, Università di Palermo, Palermo, Italy, [2]Servicio Geológico Colombiano, Observatorio Vulcanológico y Sismológico de Manizales, Manizales, Colombia, [3]Servicio Geológico Colombiano, Observatorio Vulcanológico y Sismológico de Pasto, Pasto, Colombia, [4]Servicio Geológico Colombiano, Observatorio Vulcanológico y Sismológico de Popayán, Popayán, Colombia, [5]Department of Space, Earth and Environment, Chalmers University of Technology, Gothenburg, Sweden, [6]Istituto Nazionale di Geofisica e Vulcanologia, Sezione di Palermo, Palermo, Italy

Key Points:
- A new report on volcanic gas compositions and volatile fluxes for three of the most persistently active volcanoes in the CAS is presented
- We estimate that subaerial emissions from CAS volcanoes contribute about 50% to the total subaerial CO_2 budget of the Andean Volcanic Belt
- Our work highlights the distinct magmatic CO_2/S_T signatures of Andean volcanoes, with emphasis on its northward increase and relation to along-arc variations in carbon-rich sediment input

Supporting Information:
- Supporting Information S1

Correspondence to:
J. Lages,
joaopedro.nogueiralages@unipa.it

Citation:
Lages, J., Chacón, Z., Burbano, V., Meza, L., Arellano, S., Liuzzo, M., et al. (2019). Volcanic gas emissions along the Colombian Arc Segment of the Northern Volcanic Zone (CAS-NVZ): Implications for volcano monitoring and volatile budget of the Andean Volcanic Belt. *Geochemistry, Geophysics, Geosystems*, *20*. https://doi.org/10.1029/2019GC008573

Received 17 JUL 2019
Accepted 2 OCT 2019
Accepted article online 10 OCT 2019

Abstract Studying spatial and temporal trends in volcanic gas compositions and fluxes is crucial both to volcano monitoring and to constrain the origin and recycling efficiency of volatiles at active convergent margins. New volcanic gas compositions and volatile fluxes are here reported for Nevado del Ruiz, Galeras, and Purace, three of the most persistently degassing volcanoes located in the Colombian Arc Segment of the Northern Volcanic Zone. At Nevado del Ruiz, from 2014 to 2017, plume emissions showed an average molar CO_2/S_T ratio of 3.9 ± 1.6 (S_T is total sulfur, S). Contemporary, fumarolic chemistry at Galeras progressively shifted toward low-temperature, S-depleted fumarolic gas discharges with an average CO_2/S_T ratio in excess of 10 (6.0–46.0, 2014–2017). This shift in volcanic gas compositions was accompanied by a concurrent decrease in SO_2 emissions, confirmed on 21 March 2017 by high-resolution ultraviolet camera-based SO_2 fluxes of ~2.5 kg/s (~213 t/day). For comparison, SO_2 emissions remained high at Nevado del Ruiz (weighted average of 8 kg/s) between 2014 and 2017, while Puracé maintained rather low emission levels (<1 kg/s of SO_2, $CO_2/SO_2 \approx 14$). We here estimate carbon dioxide fluxes for Nevado del Ruiz, Galeras, and Puracé of ~23, 30, and 1 kg/s, respectively. These, combined with recent CO_2 flux estimates for Nevado del Huila of ~10 kg/s (~860 t/day), imply that this arc segment contributes about 50% to the total subaerial CO_2 budget of the Andean Volcanic Belt. Furthermore, our work highlights the northward increase in carbon-rich sediment input into the mantle wedge via slab fluids and melts that is reflected in magmatic CO_2/S_T values far higher than those reported for Southern Volcanic Zone and Central Volcanic Zone volcanoes. We estimate that about 20% (~1.3 Mt C/year) of the C being subducted (~6.19 Mt C/year) gets resurfaced through subaerial volcanic gas emissions in Colombia (Nevado del Ruiz ~0.7 Mt C/year). As global volcanic volatile fluxes continue to be quantified and refined, the contribution from this arc segment should not be underestimated.

1. Introduction

Carbon (C)- and sulfur (S)-containing molecules are, after water, the two most abundant magmatic volatiles in silicate melts (Wallace et al., 2015). The exchange of these volatiles between the Earth's crust and mantle occurs primarily along subduction zones, where volatile recycling at subducted slabs results into volatile-rich magmas that degas carbon dioxide (CO_2) and sulfur dioxide (SO_2) to the atmosphere through active arc volcanoes (Aiuppa, Fischer, et al., 2017). Quantifying the arc-resolved (e.g., Hilton et al., 2002) and global arc (see a review in Burton & Sawyer, 2013) magmatic volatile fluxes is thus key to better understanding volatile cycling in and out of the planet and consequently planetary evolution over geological time (Dasgupta, 2013; Keleman & Manning, 2015).

Unfortunately, however, while the global volcanic arc S budget is relatively well characterized (e.g., Shinohara, 2013), estimates of the global arc volcanic CO_2 flux span 1 order of magnitude or more (Marty & Tolstikhin, 1998; Fischer, 2008; Burton & Sawyer, 2013; Shinohara, 2013). In contrast to SO_2, which is

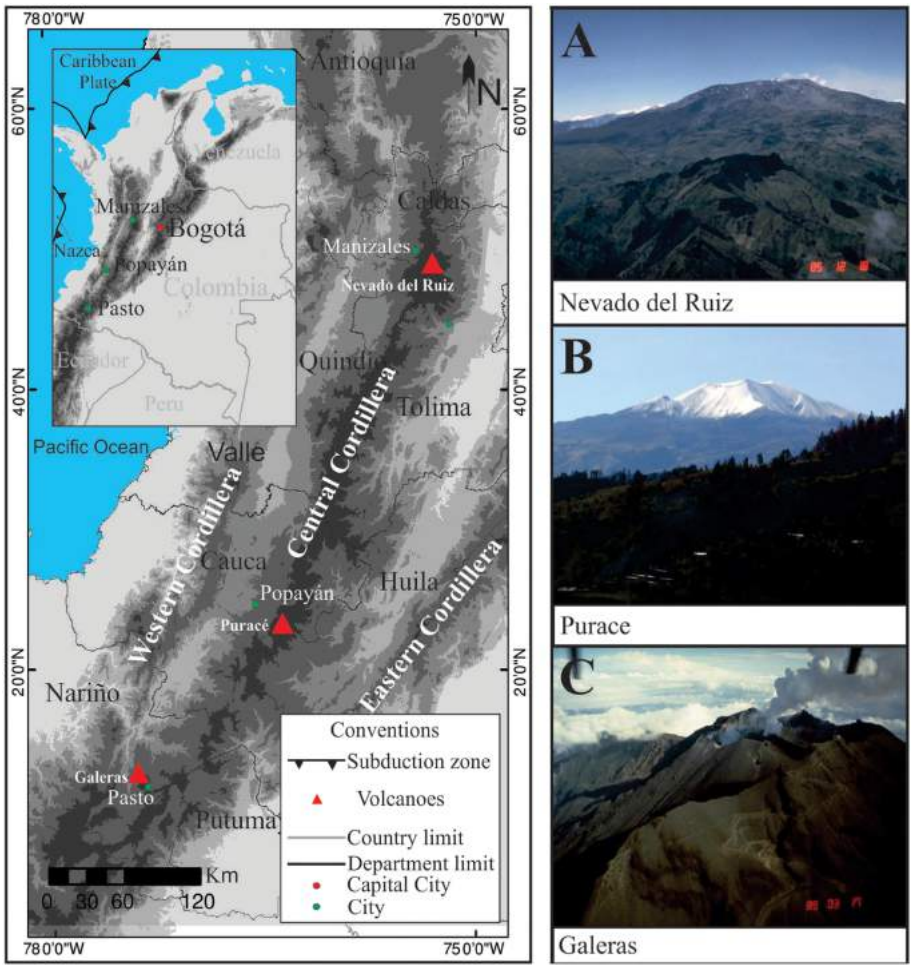

Figure 1. Map showing the location of Galeras, Puracé, and Nevado del Ruiz along the Central Cordillera of the Andes. (a**)** Nevado del Ruiz volcano; (b) Puracé volcano; and (c) Galeras (all photos from the Global Volcanism Program, 2013a, 2013b, 2013c).

scarcely present in air and effectively absorbs ultraviolet (UV) radiation (e.g., Edmonds et al., 2003; Mori & Burton, 2006; Kantzas & McGonigle, 2008; Kern et al., 2013; Carn et al., 2017), high background concentration in the atmosphere, and the presence of several absorption interferences in the infrared, complicates volcanic CO_2 remote sensing from both ground (Aiuppa et al., 2015; Queißer et al., 2018) and space (Schwandner et al., 2017). Therefore, volcanic CO_2 flux estimates are typically derived indirectly by combining measurements of SO_2 flux and of CO_2/SO_2 ratios in volcanic gases (e.g., Aiuppa et al., 2006; Shinohara et al., 2008). The latter measurements require in situ gas observations in hazardous and/or difficult to access volcanic craters, which have so far proven to be impossible for several volcano targets worldwide (Aiuppa et al., 2019), making the CO_2 budget inaccurately known for several arc segments (Shinohara, 2013), and globally (Aiuppa et al., 2019).

Here we aim at refining our current understanding of volcanic arc CO_2 budgets, by presenting novel volcanic gas information (both compositions and fluxes) for the Colombian Arc Segment (CAS). The CAS hosts 20 Holocene volcanoes (Figure 1), many of which currently show evidence of volcanic activity at the surface. While previous work has been made to characterize volatile emissions at some of these volcanoes, including Galeras (e.g., Fischer et al., 1997) and Puracé (e.g., Sturchio et al., 1993), no high-temperature volcanic gas compositions have yet been reported for Nevado de Ruiz, the most actively degassing volcano in the Andean Volcanic Belt (2005–2015; Carn et al., 2017). We here present the first volcanic gas plume results for this volcano from which, by integration with novel data for Galeras and Puracé, we derive, for the first time, the volatile (CO_2) budget for the most persistently volcanic gas emitters along the CAS. Our novel

results also open the way to a better characterization of the along-arc volcanic gas compositional trends in South America and thus to shed new light on the complex origin and recycling processes of volatiles at convergent margins (Aiuppa, Fischer, et al., 2017). Moreover, our volcanic gas results will help to establish baselines for key volcanic gas-related monitoring parameters (e.g., CO_2/SO_2 ratios; Aiuppa et al., 2017), which is critical to accurately interpret variations in geochemical precursors that may precede periods of volcanic unrest. This is especially important for volcanoes such as Galeras and Nevado del Ruiz, which in recent times have caused tremendous destruction and devastation to neighboring communities in Colombia (e.g., Voight, 1990; Voight et al., 2016).

1.1. The Colombia Arc Segment

The morphologically continuous mountain chain of the Andes persists for over 7,000 km along the western margin of South America. Volcanism here occurs in four separate regions, the Northern (NVZ), Central (CVZ), Southern, and Austral Volcanic Zones. The Colombia Arc Segment (CAS) is part of the Holocene NVZ of the Andes, which results from subduction of the 12–20 Ma Nazca Plate (slab age from Jarrard, 1986) beneath the South American Plate. This section of the volcanic arc, with an extension of approximately 530 km, hosts 20 active volcanoes located along the Central Cordillera, the highest of the three branches of the Colombian Andes (Figure 1). Twelve of them are currently classified with unrest level IV, including Puracé, in a scale for which I is accredited to on-course or eminent eruptions. Nevado del Ruiz and Galeras are classified with level III of volcanic activity, attributed to volcanoes that show frequent change on monitoring parameters of volcanic activity (Boletines Informativos, Servicio Geológico Colombiano (n. d.); https://www2.sgc.gov.co/volcanes).

Here we report new compositional and flux data from three of the main volatile emitters in the CAS, Puracé, Nevado del Ruiz, and Galeras (Figure 1). The last two are part of the DECADE initiative (https://deepcarboncycle.org/home-decade) that aims to improve estimates of global fluxes of volcanic CO_2 to the atmosphere. Nevado del Ruiz and Galeras have been identified as two of the 91 strongest volcanic SO_2 degassing in the period 2005–2015 (Carn et al., 2017). Based on satellite measurements made by the Ozone Monitoring Instrument (OMI), Carn et al. (2017) estimated the time-averaged (2005–2015) SO_2 flux for Nevado del Ruiz at 1,074 $\pm$ 1,376 t/day, making it the largest SO_2 emitter in the NVZ (Colombia and Ecuador). Over the same decade, Galeras emitted on average 218 $\pm$ 317 t/day of SO_2 (Carn et al., 2017), about half of the registered flux for this volcano prior to 2005 (450 t/day; Zapata et al., 1997; Andres & Kasgnoc, 1998).

2. Eruptive history and recent volcanic activity

2.1. Nevado del Ruiz

Nevado del Ruiz (4.892°N, 75.324°W; 5,279 m a.s.l.) is an andesitic stratovolcano located in the department of Caldas, central Colombia, near the northern end of the NVZ. Its first major eruptive period initiated 1.8 Ma ago, followed by a second eruptive stage that lasted approximately 0.6 Ma, from 0.8 to 0.2 Ma ago (Thouret et al., 1990). A summit caldera, formed around the end of the second eruptive period, has now been filled by numerous composite lava domes that characterize the present-day NdR. The modern edifice consists of a truncated cone built by lava flows propagating toward the northeastern, west-northwestern, and east-southeastern flanks. The volcano displays a glacier-covered summit surrounding the 1-km-wide, 240-m-deep Arenas crater. Over the past 11 ka, Nevado del Ruiz has explosively erupted andesitic to dacitic magmas, for a total of 12 identified eruptive stages. On 13 November 1985, a short-lived eruptive pulse of a Volcanic Explosivity Index (VEI) of 3 caused the melting of the summit ice cap and generated a sequence of deadly lahars that killed approximately 25,000 people (Hall, 1990). Explosive events associated with the currently active Arenas crater included other small occurrences nonetheless capable of creating debris avalanches, pyroclastic flows, and surges such as the ones recorded on 19 February 1845 (Thouret et al., 1990). Previous work done on the magmatic-hydrothermal system of Nevado del Ruiz (Arango et al., 1970; Giggenbach et al., 1990; Sturchio et al., 1988) suggests a strong gas-water interplay beneath the Arenas crater, with continuous release of heat and gas to the hydrothermal system by the intrusion and subsequent crystallization of magmas emplaced during the last period of major effusive activity several hundred thousand years ago (Thouret et al., 1985). These sporadic injections of high-temperature magmatic fluids from depth are thought to trigger recurrent periods of seismic unrests at Nevado del Ruiz, with plumes of water

vapor and volcanic gas reaching heights up to ~700 m above the Arenas crater that continue to be reported today by the local volcano observatory in Manizales.

2.2. Galeras

Galeras (1.221°N, 77.359°W; 4,276 m a.s.l.) is the youngest active cone of the Galeras Volcanic Complex. It is located ~60 km north of the Colombia-Ecuador border, in the department of Nariño. Over the past 1 Ma this complex has been characterized by caldera-forming eruptions, followed by the construction of active cones that produced lavas and pyroclastic flows, ranging from basaltic andesites to dacites (Calvache & Williams, 1997a, 1997b). The present-day active cone lies in the uppermost part of the sector collapse depression that occurred between 12 and 5 ka ago, during the Urcunina stage (the last eruptive stage before the formation of the present active center at the Galeras Volcanic Complex; Calvache et al., 1997a,b). It rises 150 m above the caldera floor and presents four different craters. The reactivation of the system in 1988 followed one of the four longest repose periods (1948–1988) in the last four centuries. Prior to that, most eruptive episodes, in particular those that took place in the beginning of the twentieth century (e.g., 27 August 1936), exhibited similar eruptive features, producing vertical eruptive columns, ash fall, and small pyroclastic flows (about 3–4 km long; Calvache, 1990). The reactivation of the volcanic system in 1988 was marked by increasing gas emissions and number of earthquakes. Until 1993, the volcano was almost continuously active, with a series of explosive eruptions recorded in May 1989, high levels of degassing and seismicity between 1989 and 1991, and andesitic dome emplacement between September and November 1991, which was destroyed in a series of vulcanian explosions during 1992–1993 (Stix et al., 1997). These last events are believed to have been caused by continuous pressurization of the main conduit as a result of small amounts of crystallization and cooling happening at shallow depths (Stix et al., 1993, 1997), a similar process to that described by Giggenbach et al. (1990) for Nevado del Ruiz. The same conduit dynamics are thought to be responsible for the most recent eruptive events, such as those that occurred between 2008 and 2010 (VEI 3) and more recently in January 2014 (VEI 2). Present-day gas discharges and summit activity differ from those observed in the 1990s, when degassing was concentrated in the *Deformes* and *Besolima* fumaroles, with temperatures between 200 and 500 °C (Sano et al., 1997 and Sano & Williams, 1996). Today, three main fumarolic emissions, Paisita, Chavas, and the central crater, are the main degassing sources at the closed-vent Galeras system. The temperature of the fumaroles was not directly measured due to inaccessibility to the vent areas, but visual inspection and nature of sublimates in the fumaroles' surroundings suggest near-boiling temperatures.

2.3. Puracé

Puracé (2.314°N, 76.395°W; 4,630 m a.s.l.) is a dacitic shield volcano, capped by an andesitic cone of lavas and pyroclastic deposits (Monsalve & Pulgarín, 1993), located in the department of Cauca, SW Colombia. It is the most active center in the Coconucos Volcanic Chain, a chain that comprises 15 volcanic features along a system of longitudinal and transversal regional faults, having erupted at least 12 times this century (Sturchio et al., 1988). Eruptions such as the last one recorded in the year of 1977 have produced andesitic lavas, pyroclastic flows, and surges, as well as lahars (Monsalve, 1996; Monsalve & Pulgarín, 1993). Currently, weak fumarolic activity is observed at the bottom of the main crater, whereas the main source of degassing is a fumarolic field on the outer northwest volcano's flank of temperatures as high as 135 °C.

3. Materials and Methods

Data reported in this study result from field campaigns in Colombia between 2014 and 2017. In situ fumarolic gas composition was first measured at Paisita (Galeras) on 17 October 2014, four days before the first plume measurements at Nevado del Ruiz were acquired. With support from the local observatory of Pasto (SGC-OVSP) regular MultiGAS (Multi-component Gas Analysis System; Aiuppa et al., 2005, Shinohara, 2005) surveys in Paisita took place between February and July, 2016. In March 2017, volcanic gas compositions were obtained for all three volcanoes here investigated, including Puracé and two additional fumarolic sources at Galeras (Chavas and the central crater). Finally, in July 2017, volcanic gas surveys were repeated in Galeras and Nevado del Ruiz. From then until 20 December 2017, a permanent MultiGAS station deployed at Nevado del Ruiz recorded daily volcanic gas composition data.

3.1. In Situ Volcanic Gas Measurements

We used a set of MultiGAS units to measure the in-plume concentrations of the major volcanic volatiles at the three Colombian volcanoes. Each instrument was composed of a Gascard nondispersive infrared CO_2 spectrometer from Edinburgh Sensors (accuracy, ±1.5%; calibration range of 0–3,000 ppm) and City Tech SO_2, H_2S, and H_2 electrochemical sensors with calibration ranges of 0–200, 0–100, and 0–50 ppm, respectively (repeatability, 1%). The system also included temperature (T) and relative humidity (Rh) KVM3/5 Galltec-Mela sensors. All system components and respective power sources were contained within a weather-resistant plastic case, with inlet/outlet ports to provide access to ambient air. Gas sensors were calibrated prior and following each measurement campaign at the Earth and Marine Sciences Department (DiSTeM, University of Palermo) with standard gas mixtures for CO_2 of 300 and 3,000 ppmmol (effective concentrations of 293.7 and 2,920 ppmmol, respectively), for SO_2 of 100 ppmmol (effective concentration 102.7 ppmmol), for H_2S of 40 ppmmol (38.0 ppmmol) and for H_2 of 10 ppmmol (10.0 ppmmol). In the field, volcanic gas was pumped through the in-series connected sensors, using a small pump with a flow rate of 1.8 L/min, and in-plume gas concentrations measured at a frequency of 1 Hz. Each measurement was preceded by instrument warm-up (3 min) and 2 min of ambient air flow to flush residual volcanic gas that remained trapped within the circuit.

At Nevado del Ruiz, all measurement surveys of volcanic gas composition, from 2014 and 2017, were performed at, and around, Bruma (4.90°N, −75.34°W; 4,832 m a.s.l.), a site located in the middle of a flank canyon carved by previous volcanic activity. Due to its geomorphology, the canyon channels the main vent plume downwind, over the NW flank of the edifice. Despite persistent gas emissions from the central crater, complex weather conditions (e.g., sudden shifts in wind direction) made plume capture very intermittent and compositions were obtained from rare patches of wind-blown volcanic gas. In June 2017, the gas unit was permanently installed in Bruma, approximately 2 km away from the main vent and configured to collect measurements of volcanic gas at 1 Hz in cycles of 30-min duration, separated by intervals of 6 hr (four cycles per day).

At both Galeras and Puracé, discrete MultiGAS measurements were made at close proximity to the main summit fumarolic sources. At Galeras, the volcanic gas compositional data we report on were acquired during walking traverses in and around two sparse fumarolic gas emissions (Paisita and Chavas) and at the central crater. Today the main crater of Puracé shows no evidence of persistent degassing, and measurements at this volcano were made at the *fumarola lateral*, currently the most vigorous source of volcanic gases to the atmosphere.

MultiGAS data were analyzed by selecting specific acquisition windows that showed good temporal correlation between the concentrations of volatiles species measured simultaneously (e.g., Aiuppa et al., 2014; Tamburello et al., 2015). Given the pressure difference between calibration (P = 1,013 mbar) and measurement (P = 577–610 mbar) site, manufacturer pressure corrections (0.015% signal per hPa for SO_2 and 0.008% signal per hPa for H_2S) were estimated at ≤0.2% effect on the calculated x/SO_2 ratios across our data set. Therefore, such trivial variances have not been considered, and all ratios reported are uncorrected. CO_2 readings were automatically pressure compensated by the nondispersive infrared spectrometer. Cross-sensitivity effects of SO_2 on the H_2S sensor were estimated at 14.5% during calibration, and corrections were applied during data processing to calculate interference-corrected H_2S concentrations in the gas plume. A scatter plot of the CO_2 versus SO_2 concentrations (in ppmv) is shown in Figure 2a, where the corresponding averaged CO_2/SO_2 ratio in that temporal interval is calculated from the slope of the best fit regression line (dashed blue line). The same procedure was applied to calculate in-plume relative abundances of other volatile species such as H_2S/SO_2 and H_2O/CO_2. CO_2 and H_2O concentration ratios were estimated after subtraction of background-air concentration ratios acquired at plume-free areas. H_2O concentration ratios were calculated using measurements of T, P, and Rh and the Arden Buck equation (Tamburello, 2015). For each fit window, the peak SO_2 concentration was used to trace the intensity of the gas plume and is here considered as an analog of measurement quality. Reported composition averages (e.g., x/SO_2 and mol%) are, therefore, based on predetermined weights assigned to each MultiGAS measurement by the maximum amount of SO_2 recorded by the instrument for a given acquisition window.

3.2. UV Camera Measurements

We used a dual UV camera system (Tamburello, Kantzas, McGonigle, Aiuppa, & Gaetano, 2011) for survey-type SO_2 flux measurements at Nevado del Ruiz and Galeras. The system consisted of two co-aligned

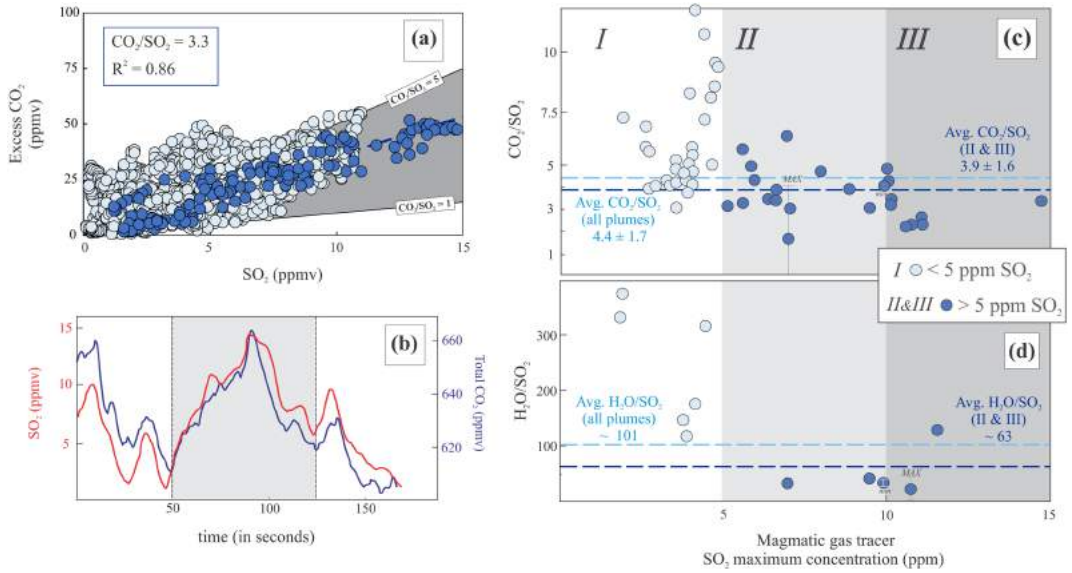

Figure 2. (a) Nevado del Ruiz CO_2 versus SO_2 (ppmv) scatterplot showing an example of an acquisition window with all data in light blue and individual data points used to determine the slope of the best fitting linear regression line (dotted dark blue line, $R^2 = 0.86$). Gray area demarks the field of $5 \geq CO_2/SO_2 \geq 1$; (b) Acquisition window showing the concentration time series of SO_2 and excess CO_2 (after atmospheric background subtraction) in ppmv. Gray area corresponds to the time window selected to calculate CO_2/SO_2 ratio shown in (a). (c and d) CO_2/SO_2 and H_2O/SO_2 versus SO_2 maximum concentration (in ppm) shown for all plume categories, from I ($0 < SO_2 < 5$ ppm; light blue data points) to II and III ($5 < SO_2 < 15$ ppm; dark blue data points). To single out the "magmatic" CO_2/SO_2 and H_2O/SO_2 ratios, Category I type plumes were not considered in the average estimates marked by the dark blue dashed line. The average of our entire data set is represented by the light blue dashed line.

cameras used simultaneously to measure incident radiation through filters centered at 310 (effective SO_2 absorption region) and 330 nm (outside of the absorption range). Observations at both volcanoes were conducted between 7 and 9 a.m. (GMT −5; period with the lowest cloud coverage) at distances of 2.2 and 2.5 km for Nevado del Ruiz and 0.5 km for Galeras. Measurement sites were selected so as to grant a clear view of the gas plume, with blue sky in the background and the volcanic edifice framed within the acquisition window. The JAI CM-140 GE-UV dual-set UV cameras are fitted with a Sony ICX407BLA UV-enhanced CCD array sensor (10 bit, 1,392 × 1,040 pixels) and equipped with an electronic shutter architecture and GiGE Vision interface. Two quartz lenses (UKA optics UV1228CM, focal length 12 mm) provided a horizontal field of view of ~37°, while the two band-pass filters (Edmund 310nm CWL and 330nm CWL, 10-nm full width at high maximum) were placed between the lenses and the charge-coupled device array to avoid variations in wavelength response (Kern et al., 2013). Before acquisition, the UV camera system was calibrated using three calibration cells of known SO_2 concentrations (203, 998, and 1,861, ppm m), which allowed the calibration of the qualitative measured apparent absorbance (Kantzas et al., 2010; Lübcke et al., 2012). The system was powered by a 12-V lithium battery. With this setup, sequential images of the plume were captured at ~0.5-Hz rate. For image acquisition and processing we used Vulcamera, a stand-alone code specifically designed for measuring SO_2 fluxes using UV cameras (Tamburello, Kantzas, McGonigle, & Aiuppa, 2011). Cross correlation of two integrated column amounts time series (obtained along two closely spaced parallel sections, perpendicular to the plume) and absorbance for each camera pixel were calculated using the methodology of Kantzas et al. (2010; integrated in the Vulcamera software) and used to finally derive plume speed.

3.3. NOVAC Measurements

For Nevado del Ruiz and Galeras, in addition to our survey-type UV camera results, we also used the systematic SO_2 flux records obtained by the local network of UV scanning spectrometers of NOVAC, the global Network for Observation of Volcanic and Atmospheric Change (Galle et al., 2003, 2010). At Nevado del Ruiz, data from five NOVAC scanning mini-differential optical absorption spectroscopy (DOAS; Johansson et al.,

2009) instruments were combined with meteorological information to derive daily statistics of total SO_2 emissions. The use of five scanners allows effective plume capturing for virtually any plume transport direction. At both Galeras and Puracé, one scanning unit was available, and data from these instruments are considered below.

Each plume scan is composed of 51 radiance spectra taken across the scanning plane at steps of 3.6°. Flat and conical scan modes were used. The first comprises a scan performed from horizon to horizon along a vertical surface passing zenith, whereas for the conical scanner, with an opening angle of 60°, a more efficient scan geometry is obtained, providing results under larger deviation in wind direction. Each scan sequence starts with optimization of the exposure time for a spectrum taken in the position closest to zenith (limited to 1,000 ms). This exposure time is kept constant for all measurements in the same scan. Usually, 15 spectra are averaged at each position to improve the signal-to-noise ratio. An additional dark-current/offset spectrum is measured on each scan, with the fore-optics facing the shadowed nadir position of the scanner. Data are saved in situ and then transmitted to the observatory for real-time evaluation. For SO_2 calculations, the plume speed is obtained from the ECMWF/ERA-Interim database (Dee et al., 2011), whereas plume direction and altitude is obtained by triangulation of consecutive scan measurements. Daily averages are estimated by simply calculating the arithmetic mean of all valid scans recorded on a single day. The uncertainties reported (1σ of the daily mean) have been factored in the weighted SO_2 flux yearly average (2014–2017 for Galeras and Nevado del Ruiz), in order to give more relevance to days for which data were acquired more consistently.

Detailed information on retrieval of relative SO_2 slant column densities, SO_2 vertical column densities, SO_2 flux and plume parameters, statistics, and uncertainties associated with each measurement (including uncertainties related to wind speed retrievals from the ECMWF-ERA5 meteorological model) are provided as supporting information Text S1.

4. Results

4.1. Gas Composition

4.1.1. Nevado del Ruiz

At Nevado del Ruiz, due to high volcanic activity levels recorded throughout this investigation, proximal crater areas have remained inaccessible, thus hampering near-vent in-plume observations. Our measurements at Bruma are thus representative of a distal, aged 215- to 590-s plume, depending on highly variable wind speed (daily average estimates ranging from 3.5 to 9.5 m/s) plume. Due to temporal variations in plume transport direction and speed, the plume was variably diluted while our measurement point was fumigated, so that atmospheric dilution upon transport is responsible for the large variations in gas concentrations detected by the MultiGAS. Sulfur dioxide concentrations spanned from <1 to ~15 ppm, while background air-corrected CO_2 concentrations varied from <1 to ~50 ppm (Figure 2a). Magmatic H_2O was more episodically detected above the atmospheric backgrounds and ranged from <10 to ~2,950 ppmv. H_2S was rarely detected above the 14.5% cross-sensitivity to SO_2 and showed maximum concentrations of ~0.30 ppmv, while MultiGAS measurements recorded H_2 concentrations up to 5 ppmv.

The derived volatile ratios (in the form of x/SO_2 ratios; where x is H_2O, CO_2, H_2S, or H_2) at Nevado de Ruiz are listed in Table 1a. All x/SO_2 plume ratios were obtained in measurement windows where strong positive covariations ($R^2 > 0.6$) were observed between SO_2 and other volatiles (see example in Figure 2b) and correspond to the gradients of the best fit regression lines in the scatterplots (e.g., Figure 2a). The interference-corrected H_2S/SO_2 ratio and the H_2/SO_2 ratio showed small variations throughout the course of the investigation, with mean values of 0.1 ± 0.005 and 0.2 ± 0.1 (uncertainties correspond to one standard deviation on the average, here and below), while CO_2/SO_2 and H_2O/SO_2 ratios varied more widely, as discussed below.

The derived CO_2/SO_2 molar ratios (Table 1a and Figure 2c) are grouped into three different categories depending on the peak SO_2 concentration ($SO_{2\ MAX}$) detected during each measurement interval: (I) $SO_{2\ MAX} < 5$; (II) $5 \leq SO_{2\ MAX} < 10$; and (III) $SO_{2\ MAX} \geq 10$ (in ppm). The more scattered category I CO_2/SO_2 ratio data (Figure 2c, in light gray) potentially reflect either higher analytical uncertainties on the derived volcanic CO_2 concentrations in dilute plume conditions or the presence of other CO_2

Geochemistry, Geophysics, Geosystems

10.1029/2019GC008573

Table 1

x/SO_2 Molar Ratios Measured by MultiGAS and Gas Composition of (a) Nevado del Ruiz, (b) Galeras, and (c) Puracé With Error Represented as 1σ From the Weighted Daily Mean

Date	Molar ratio CO_2/SO_2	Error (1σ)	Molar ratio H_2S/SO_2	Error (1σ)	Molar ratio H_2/SO_2	Error (1σ)	Molar ratio H_2O/SO_2	Error (1σ)	SO_2 MAX	Composition (mol%)									
										SO_2	(1σ)	CO_2	(1σ)	H_2S	(1σ)	H_2	(1σ)	H_2O	(1σ)
(a) Nevado del Ruiz																			
21 Oct 14	2.6	0.5	0.12	<0.01	0.08	<0.01	26	10	11.0	3.4	n/d	8.6	1.7	0.4	0.0	0.3	0.0	87.3	34.2
22 Oct 14	4.2	1.5	0.11	0.01	0.07	0.02	—	—	3.9	—	—	—	—	—	—	—	—	—	—
29 Mar 17	5.4	5.3	0.14	<0.01	0.45	0.21	323	48	4.4	0.3	n/d	1.7	1.6	0.0	0.0	0.1	0.1	97.9	14.5
1 Jul 17	4.1	2.5	0.20	<0.01	0.21	<0.01	—	—	3.4	—	—	—	—	—	—	—	—	—	—
2 Jul 17	5.4	2.0	0.19	<0.01	0.18	<0.01	—	—	3.8	—	—	—	—	—	—	—	—	—	—
4 Jul 17	9.6	3.8	0.18	<0.01	0.17	<0.01	—	—	4.8	—	—	—	—	—	—	—	—	—	—
11 Sep 17	7.2	2.8	0.14	<0.01	0.18	<0.01	164	41	4.0	0.6	n/d	4.2	1.6	0.1	0.0	0.1	0.0	95.1	237.2
14 Oct 17	1.6	1.3	0.12	<0.01	0.20	0.1	—	—	7.0	—	—	—	—	—	—	—	—	—	—
15 Oct 17	8.2	7.1	0.13	<0.01	0.24	<0.01	—	—	6.0	—	—	—	—	—	—	—	—	—	—
16 Oct 17	4.3	0.2	0.13	<0.01	0.12	<0.01	—	—	10.0	—	—	—	—	—	—	—	—	—	—
17 Oct 17	3.3	1.4	0.12	<0.01	0.09	<0.01	127	38	14.8	0.8	n/d	2.5	1.1	0.1	0.0	0.1	0.0	96.6	28.8
31 Oct 17	3.9	4.9	0.10	<0.01	0.19	0.2	—	—	2.9	—	—	—	—	—	—	—	—	—	—
1 Nov 17	4.5	0.7	0.14	<0.01	0.21	0.01	—	—	3.5	—	—	—	—	—	—	—	—	—	—
12 Nov 17	4.4	3.1	0.10	0.01	0.21	0.10	—	—	5.6	—	—	—	—	—	—	—	—	—	—
14 Nov 17	5.0	1.1	0.14	<0.01	0.21	0.08	—	—	4.0	—	—	—	—	—	—	—	—	—	——
22 Nov 17	4.0	0.9	0.14	<0.01	0.11	<0.01	—	—	6.6	—	—	—	—	—	—	—	—	—	—
23 Nov 17	5.5	1.8	0.16	<0.01	0.20	0.09	—	—	2.7	—	—	—	—	—	—	—	—	—	—
26 Nov 17	5.4	1.4	0.12	<0.01	0.12	<0.01	—	—	8.0	—	—	—	—	—	—	—	—	—	—
4 Dec 17	3.9	1.5	0.15	0.02	0.21	0.04	—	—	6.4	—	—	—	—	—	—	—	—	—	—
5 Dec 17	3.0	0.0	0.13	0.01	0.16	0.02	—	—	7.0	—	—	—	—	—	—	—	—	—	—
6 Dec 17	3.1	0.0	0.13	<0.01	0.19	<0.01	41	22	10.1	2.2	n/d	6.9	0.0	0.3	0.0	0.4	0.0	90.2	48.3
7 Dec 17	4.1	0.0	0.13	<0.01	0.14	<0.01	32	23	9.9	2.7	n/d	10.8	0.0	0.3	0.0	0.4	0.0	85.9	60.3
15 Dec 17	5.0	0.2	0.13	<0.01	0.17	<0.01	—	—	7.5	—	—	—	—	—	—	—	—	—	—
16 Dec 17	3.9	1.4	0.15	<0.01	0.24	<0.01	—	—	4.0	—	—	—	—	—	—	—	—	—	—
17 Dec 17	7.1	4.1	0.13	0.02	0.19	0.03	377	102	1.9	0.3	n/d	1.8	1.1	0.0	0.0	0.1	0.0	97.8	26.5
19 Dec 17	4.1	1.7	0.18	<0.01	0.33	<0.01	—	—	3.5	—	—	—	—	—	—	—	—	—	—
20 Dec 17	4.9	1.9	0.14	<0.01	0.25	<0.01	—	—	4.6	—	—	—	—	—	—	—	—	—	—
(b) Galeras																			
17 Oct 14	6.0	1.2	0.55	0.04	0.04	0.01	26	13	61.6	3.0	n/d	21.0	4.0	1.6	0.1	0.1	<0.1	74.3	36.0
26 Feb 16	13.4	5.4	—	—	—	—	—	—	27.3	—	—	—	—	—	—	—	—	—	—
29 Feb 16	15.3	4.2	—	—	—	—	—	—	56.5	—	—	—	—	—	—	—	—	—	—
27 Apr 16	14.2	1.3	—	—	—	—	—	—	73.6	—	—	—	—	—	—	—	—	—	—
31 May 16	14.6	1.9	—	—	—	—	—	—	15.1	—	—	—	—	—	—	—	—	—	—
13 Jul 16	13.3	3.7	—	—	—	—	—	—	10.8	—	—	—	—	—	—	—	—	—	—

Geochemistry, Geophysics, Geosystems

10.1029/2019GC008573

Table 1
(continued)

Date	Molar ratio CO_2/SO_2	Error (1σ)	Molar ratio H_2S/SO_2	Error (1σ)	Molar ratio H_2/SO_2	Error (1σ)	Molar ratio H_2O/SO_2	Error (1σ)	SO_2 MAX	Composition (mol%)									
										SO_2	(1σ)	CO_2	(1σ)	H_2S	(1σ)	H_2	(1σ)	H_2O	(1σ)
18 Jul 16	10.8	1.5	—	—	—	—	—	—	10.6	—	—	—	—	—	—	—	—	—	—
21 Mar 17																			
Paisita	87.3	17.4	1.6	0.2	—	—	412	71.1	5.4	0.2	n/d	21.0	4.2	0.3	0.1	—	—	78.4	13.5
Chavas	5.4	0.8	2.3	0.2	1.2	0.4	327	8	5.1	0.3	n/d	1.6	0.2	0.7	0.0	0.4	0.1	97.0	2.4
Central crater	93.8	6.2	2.4	0.4	3.1	0.6	1951	486	4.9	0.1	n/d	4.8	0.3	0.1	0.0	0.2	0.0	94.9	23.7
13 Jul 17																			
Paisita	38.5	2.7	1.5	0.0	—	—	155	2	6.3	0.5	n/d	24.5	1.7	0.8	0.0	—	—	74.2	1.2
Chavas	41.7	0.9	0.9	0.1	—	—	98	<0.1	4.7	0.7	n/d	41.8	0.9	0.7	0.1	—	—	56.8	0.0
Central crater	33.6	13.7	1.2	0.1	—	—	264	16	3.0	0.3	n/d	12.6	5.1	0.4	0.0	—	—	86.6	5.3
14 Jul 17																			
Central crater	33.6	8.0	1.3	0.2	—	—	131	31	2.2	0.6	n/d	25.1	6.0	0.8	0.1	—	—	73.5	17.3
(c) Puracé																			
23 Mar 17	14.0	2.3	0.4	0.2	0.3	0.2	165	47	14.4	0.6	n/d	7.7	1.9	0.2	0.1	0.2	0.1	91.3	25.7
Hydrothermal springs						Agua Herbiendo				—	—	30.1	3.8	0.9	0.0	—	—	69.0	11.3
						Poco Azul				—	—	50.5	12.7	0.5	0.1	—	—	49.0	17.3
						San Juan de Puracé				—	—	89.9	8.5	1.0	0.2	—	—	9.1	3.6

Note. MultiGAS = Multi-component Gas Analysis System; n/d = no data.

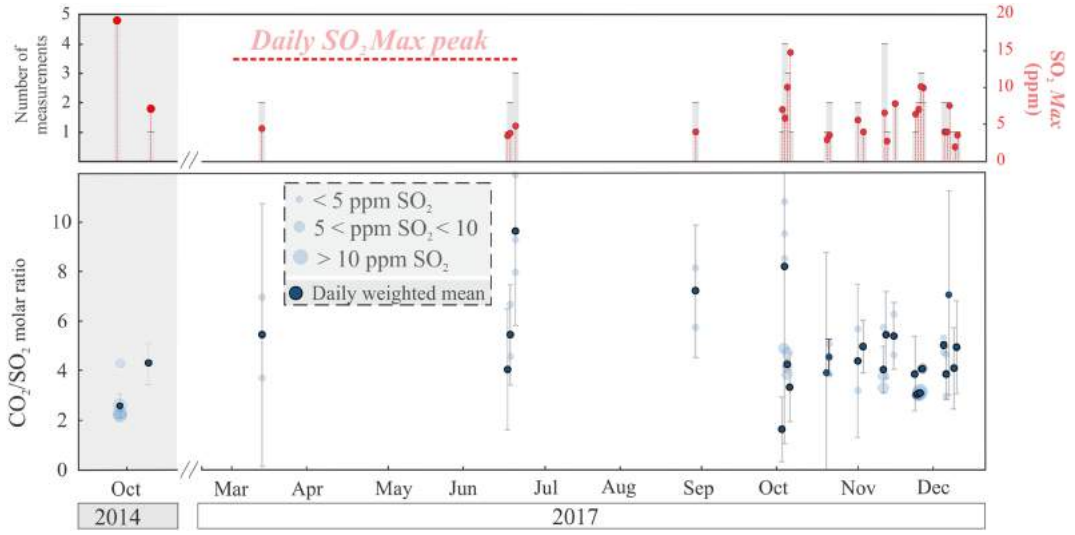

Figure 3. (a) Light grey bars indicate the number of compositional measurements used to calculate weighted daily means, while red closed circles represent the maximum SO_2 peak concentration (in ppm) recorded for each day. (b) CO_2/SO_2 time series for Nevado del Ruiz (October 2014 and March–December 2017); light blue bubble sizes are proportional to the maximum SO_2 concentration (in ppm) recorded for any given MultiGAS measurement, while dark blue closed circles symbolize weighted daily CO_2/SO_2 averages.

sources (in addition to the magmatic plume) and should thus be considered with caution in the analysis of compositional temporal trends (Figure 3b). We thus used the corresponding SO_2 peak concentration (Figure 3a) to estimate the daily CO_2/SO_2 weighted daily means, which were calculated by weighting each compositional measurement by the SO_2 peak concentration recorded during individual acquisition windows, as explained above.

On our explorative surveys of 21 and 22 October 2014, the unit ran for about 2 and 0.5 hr, respectively. Measurements on October 21 yielded CO_2/SO_2 averages of 4.2 ± 3.0 and 2.3 ± 0.1 for Categories II and III data, respectively, resulting in a daily CO_2/SO_2 weighted mean of 2.6 ± 0.5 for that day. On 22 October a more diluted plume signal ($SO_{2\ MAX}$ of 3.8 ppm) recorded an CO_2/SO_2 average of 4.2 ± 3.1. Using the same scatterplot approach (e.g., Figure 2a), H_2S/SO_2, H_2/SO_2, and H_2O/SO_2 ratios were also derived in October 2014, with obtained averages of 0.1, 0.1, and 25.7, respectively. From these compositional measurements in-plume molar proportions of 87.3 mol% H_2O, 8.6 mol% CO_2, 3.4 mol% SO_2, 0.4 mol% H_2S, and 0.3 mol% H_2 were derived in October 2014 for Nevado del Ruiz (Table 1a).

Following the same measurement routine, in March 2017, our unit measured continuously for approximate 3.5 hr in the same location. Sulfur dioxide concentrations exceeded background levels to a maximum of 4.5 ppmv, and very sparse volcanic CO_2 peaks (as high as 889 ppmv) revealed a highly diluted plume (Category I) with an CO_2/SO_2 average of 5.4 ± 5.3, similar to the results obtained in 2014 under similar measurement conditions (Figures 3a and 3b). The plume exhibited a more H_2O-rich composition (H_2O ~97.9 mol%) than in 2014, and the H_2/SO_2 ratio was also ~5 times higher (0.5 ± 0.2; Table 1a).

In July to December 2017, Category III measurements showed slightly higher CO_2/SO_2 ratios (mean, 3.2 ± 0.1) than in previous observational periods (Figure 3b). Category I and II plumes' CO_2/SO_2 averages remained higher than observed in denser (Category III) plumes, with 5.5 ± 3.2 and 4.3 ± 2.4 averages, respectively (individual CO_2/SO_2 ratios and daily means are shown in the time series of Figure 3). Magmatic H_2O signals, when distinguishable from the atmospheric background, yielded widely variable H_2O/SO_2 ratios (32–377) in July–December 2017, but Category II and III plumes converged to averaged magmatic CO_2/SO_2 and H_2O/SO_2 ratios of 3.9 ± 1.6 and 63 ± 45, respectively (Figure 2d). From the data above, the time-averaged plume composition in 2017 was thus estimated at 91.7 mol% H_2O, 6.0 mol% CO_2, 1.8 mol% SO_2, 0.2 mol% H_2S and 0.2 mol% H_2.

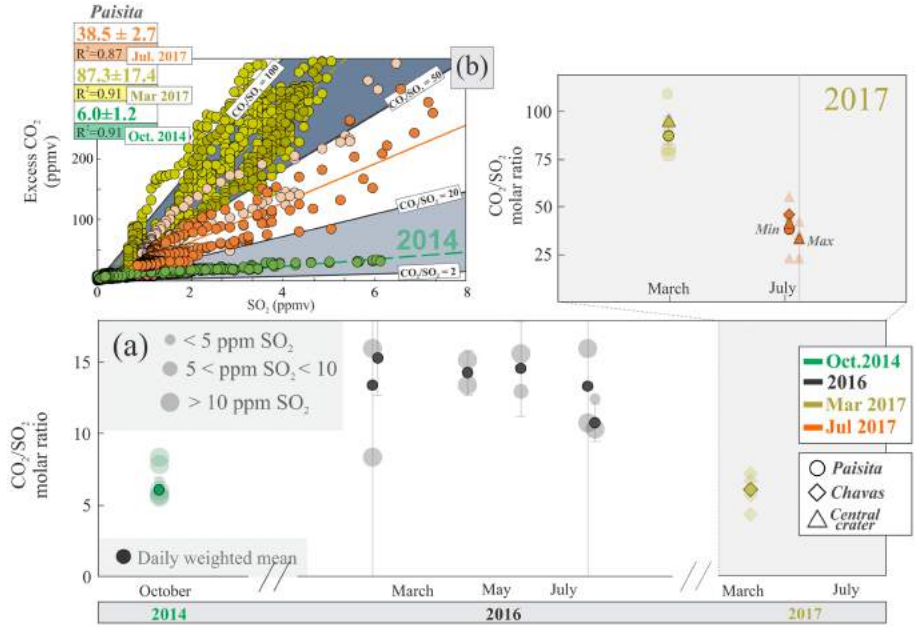

Figure 4. Galeras: (a) CO_2/SO_2 time series for Galeras (October 2014, in green; February–July 2016, in dark gray; March 2017, in olive drab; and July 2017, in orange). Light gray area delimitates the 2017 period, with inset from March to July, and shaded red bubble sizes are proportional to the maximum SO_2 amount (in ppm) recorded by each MultiGAS measurement, while dark colors symbolize weighted daily CO_2/SO_2 averages. (b) CO_2 versus SO_2 (ppmv) scatterplots of concentration ratios at Paisita from October 2014 (green), March (olive drab), and July (orange) 2017, with respective least squares sregression lines.

4.1.2. Galeras

Three emission sources, Paisita, Chavas, and the central crater, have been actively degassing at Galeras since 2014. Our results identify large temporal (at each site) and spatial (from one site to another) variations in gas composition (Table 1b). All daily CO_2/SO_2 averaged ratios, and associated errors, are shown in the time series of Figure 4a.

The first MultiGAS survey in October 2014 at Galeras was restricted to the Paisita fumarole only. This yielded a CO_2/SO_2 ratio average of 6.0 ± 1.2 (Figures 4a and 4b, in green). Sulfur dioxide was the prevalent S species (H_2S/SO_2 molar ratios of 0.6 ± 0.1), and the H_2O/CO_2 ratio averaged at ~24, yielding an averaged plume composition of ~74.3 mol% H_2O, 21.0 mol% CO_2, 3.0 mol% SO_2, 1.6 mol% H_2S, and 0.1 mol% H_2.

From February to July 2016, despite the high SO_2 concentrations recorded in the gas plume (as high as 74 ppmv), CO_2/SO_2 molar ratios at Paisita increased to 14.2 ± 1.1 (6-month-period average; Figure 4a). This increase was even more pronounced in March 2017, when the CO_2/SO_2 ratio increased at both Paisita (Figure 4b, in olive drab) and the central crater (87.3 ± 17.4 and 93 ± 6.2, respectively; Figure 4a, inset). Conversely, Chavas exhibited lower CO_2/SO_2 of 5.4 ± 0.8, similar to those observed at Paisita in 2014 (Figure 4).

Volcanic gas measurements in July 2017 confirmed a high CO_2/SO_2 ratio signature at all emission sources (Paisita, 38.5 ± 2.7; central crater, 33.6 ± 13.6; Chavas, 41.7 ± 0.9 on 13 July; central crater, 33.6 ± 8.0 on 14 July) as plotted in the inset of Figure 4a (Figure 4b shows the scatterplot of CO_2 versus SO_2 in orange for Paisita in July for comparison with previous measurements). High H_2O/SO_2 ratios were also observed at all vents (154.7 ± 2.4, 97.8 ± 0.1, and 264.3 ± 16.0 for Paisita, Chavas, and the central crater, respectively), suggesting a SO_2-poor composition, which is also consistent with a sensible increase in the H_2S/SO_2 ratios (0.6 in 2014 to as high as 2.3 in 2017). Based on these ratios, the plume compositions in July 2017 were derived at 74.3 mol% H_2O, 24.5 mol% CO_2, 0.5 mol% SO_2, 0.8 mol% H_2S, and 0.1 mol% H_2 (Paisita); 56.8, 41.8, 0.7, 0.7, and 0.1 (Chavas); and 86.6, 12.6, 0.3, 0.4, and 0.1 (central crater; Table 1b).

4.1.3. Puracé

Measurements in the lateral fumarole of Puracé (135 °C) yielded an in-plume CO_2/SO_2 ratio average of 14.0 ± 2.3 during the measurements performed on 23 March 2017 (Table 1c). The H_2O/CO_2 ratio was low

(average 10.7 ± 2.8), and the in-plume composition was estimated at 91.3 mol% H_2O, 7.7 mol% CO_2, 0.6 mol % SO_2, 0.3 mol% H_2S, and 0.2 mol% H_2. A few low-temperature peripheral gas emissions were also analyzed, yielding the following gas compositions: (i) Agua Herbiendo (59 °C), 30.1 mol% H_2O, 69.0 mol% CO_2, and 0.9 mol% H_2S; (ii) Poco Azul (85 °C), 50.5 mol% H_2O, 49.0 mol% CO_2, and 0.5 mol% H_2S; and (iii) San Juan de Puracé (34 °C), 89.9 mol% H_2O, 9.1 mol% CO_2, and 1.0 mol% H_2S. These fumaroles are thus enriched in CO_2, as typical of low-temperature gas discharges at the periphery of active volcanoes.

Daily averaged composition estimates and associated errors (±1σ of the daily mean) for Nevado del Ruiz, Galeras, and Purace are reported individually in Tables 1a–1c.

4.2. SO_2 Fluxes

On each of our MultiGAS observation days (Figure 3), the Nevado del Ruiz scanning-DOAS NOVAC system was regularly in operation and outputted the daily averaged SO_2 fluxes listed in Table 2a and graphically illustrated in Figure 5a. In 2014, for both days of acquired MultiGAS data (21 and 22 October), the SO_2 flux averaged 33 and 13 kg/s, respectively (Table 2a). From March to December 2017, the SO_2 flux ranged between 3 and ~35 kg/s, with an estimated weighted SO_2 flux average of ~8 kg/s (arithmetic mean of ~13 kg/s; see section 3.3 for details on average estimates). For comparison, measurements made on 1 and 4 July 2017 between 7 and 9 a.m. GMT −5 using the dual UV camera system, although restricted to acquisition windows limited to short periods of cloud-free conditions (~6 and ~18 min, respectively), yielded SO_2 fluxes of 21 ± 7 and 11 ± 3 kg/s (Table 2a1). These were higher and more variable than the daily averaged NOVAC-based SO_2 fluxes for the two days (4.0 and 4.4 kg/s for 1 and 4 July, respectively), despite the similar average plume speed estimates used to retrieve SO_2 outputs from both methods (~9.4 m/s for NOVAC and ~8.5 m/s for the UV camera), implying that UV camera observations may have captured short-lived phases of elevated degassing. Still, the averaged SO_2 flux for the two UV camera measurements (~16 kg/s) is well within the range of the NOVAC SO_2 outputs in 2017 (Figure 5).

The SO_2 flux oscillated between ~ 5 and 6 kg/s at Galeras (NOVAC) during our 2014 MultiGAS survey (Table 2b). In 2016 (February to July), the SO_2 flux ranged between 3 and 9 kg/s (average of ~5 kg/s), and, in 2017, no SO_2 was detected from NOVAC, suggesting a drop in SO_2 emissions that is well consistent with our MultiGAS-based compositional data (cf. section 4.1.2). However, the near-vent dual UV camera measurements performed on 21 March were well able to detect the SO_2 emissions from the volcano and to distinguish the individual SO_2 contributions from Paisita, Chavas, and the central crater (Figure 6). Acquisition windows with clear atmospheric background for all three sources were again restricted in time (11–14 min in temporal intervals between 7 and 8 a.m. GMT −5) but allowed the estimation of weighted SO_2 fluxes of 0.4 ± 0.4 ($<0.1_{[min]}$–$1.29_{[max]}$), 1.3 ± 0.6 ($<0.1_{[min]}$–$2.2_{[max]}$), and 0.8 ± 0.5 ($0.7_{[min]}$–$1.20_{[max]}$) for Paisita, Chavas, and the central crater, respectively (Table 2b1). Due to highly variable wind conditions during the acquisition period, our reported weighted means consider only fluxes estimated from plume speed values within 1σ of the mean. Values outside of this range are likely to overestimate SO_2 flux outputs and are uncharacteristic of the overall degassing pattern of all three individual subaerial discharges. The total SO_2 flux was thus 2.5 ± 1.5 kg/s, slightly lower than the 2014–2016 NOVAC records.

On 23 March 2017 the NOVAC scanning DOAS at Puracé derived an SO_2 flux of 0.1 ± 0.1 kg/s (Table 2c). The SO_2 flux remained low throughout the course of this investigation (March to December 2017).

5. Discussion

5.1. Magmatic versus Hydrothermal Gas Compositions

Our measurements here supply new information to the (currently limited) existing knowledge on the volcanic gas signature of the CAS-NVZ. The gas results for the three volcanoes are summarized and illustrated in the CO_2-S_T*5-H_2O/10 triangular plots of Figure 7 and 8.

To the best of our knowledge, our observations represent the first ever results obtained for the major element composition of the Nevado del Ruiz volcanic plume, the strongest source of SO_2 in the NVZ (Carn et al., 2017). Previous volcanic gas information on the volcano was limited to a few analyses of low-temperature (82–103 °C) hydrothermal steam vents and fumaroles collected in the crater area and along the volcano's flanks in the months following the lethal 13 November 1985 eruption (Giggenbach et al., 1990; Figures 7a

Geochemistry, Geophysics, Geosystems

10.1029/2019GC008573

Table 2
Inferred Flux Range of Each Species Based on SO_2 Flux Estimates From NOVAC: (a) Nevado del Ruiz, (b) Galeras, and (c) Puracé

Date	H_2O in kg/s (t/day)	σ	CO_2 in kg/s (t/day)	σ	SO_2 in kg/s (t/day)	σ	H_2S in kg/s (t/day)	σ	H_2 in kg/s (t/day)	σ
(a) Nevado del Ruiz—Volatile flux estimates derived from SO_2 flux daily averages (NOVAC)										
21 Oct 14	238 (20,582)	144 (12,449)	58 (4,893)	29 (2,492)	33 (2,843)	15 (1,312)	2.1 (180)	1.0 (83)	(8)	(3)
22 Oct 14	—	—	38 (3,291)	25 (2,157)	13 (1,129)	7 (623)	0.8 (68)	0.4 (38)	(2)	(2)
29 Mar 17	654 (56,536)	1060 (91,589)	27 (2,328)	51 (4,389)	7 (623)	12 (1,005)	0.5 (47)	0.9 (75)	(9)	(15)
1 Jul 17	—	—	11 (953)	15 (1,312)	4 (342)	5 (423)	0.4 (37)	0.5 (45)	(2)	(3)
2 Jul 17	—	—	—	—	—	—	—	—	—	—
4 Jul 17	—	—	29 (2,488)	28 (2,392)	4 (376)	4 (329)	0.4 (37)	0.4 (32)	(2)	(2)
11 Sep 17	143 (12,359)	377 (32,553)	15 (1,329)	14 (1,224)	3 (269)	3 (226)	0.2 (20)	0.2 (17)	(1)	(1)
14 Oct 17	—	—	9 (755)	9 (788)	8 (678)	5 (444)	0.5 (44)	0.3 (29)	(4)	(3)
15 Oct 17	—	—	139 (12,042)	147 (12,691)	25 (2,143)	15 (1,274)	1.8 (153)	1.1 (91)	(16)	(9)
16 Oct 17	—		35 (3,004)	14 (1,239)	12 (1,029)	5 (422)	0.8 (69)	0.3 (28)	(4)	(2)
17 Oct 17	690 (59,611)	711 (61,458)	44 (3,820)	47 (4,096)	19 (1,668)	19 (1,647)	1.2 (104)	1.2 (102)	(5)	(5)
31 Oct 17	—	—	95 (8,192)	125 (10,771)	35 (3,055)	14 (1,246)	2.0 (170)	0.8 (69)	(18)	(25)
1 Nov 17	—	—	93 (8,019)	64 (5,521)	30 (2,570)	20 (1,722)	2.2 (188)	1.5 (126)	(17)	(11)
12 Nov 17	—	—	81 (6,983)	85 (7,304)	27 (2,316)	21 (1,783)	1.4 (120)	1.1 (93)	(15)	(14)
14 Nov 17	—	—	49 (4,195)	28 (2,385)	14 (1,230)	8 (649)	1.1 (92)	0.6 (48)	(8)	(5)
22 Nov 17	—	—	42 (3,600)	34 (2,955)	15 (1,297)	12 (1,021)	1.6 (96)	0.9 (76)	(4)	(3)
23 Nov 17	—	—	70 (6,080)	48 (4,180)	19 (1,623)	11 (986)	0.7 (141)	1.0 (86)	(10)	(8)
26 Nov 17	—	—	40 (3,460)	26 (2,231)	11 (934)	6 (555)	0.5 (58)	0.4 (34)	(3)	(2)
4 Dec 17	—	—	30 (2,609)	23 (2,009)	11 (983)	8 (651)	0.9 (80)	0.6 (54)	(7)	(4)
5 Dec 17	—	—	18 (1,544)	16 (1,354)	9 (746)	8 (654)	0.6 (50)	0.5 (44)	(4)	(3)
6 Dec 17	110 (9,476)	95 (8,184)	20 (1,765)	14 (1,196)	10 (830)	7 (562)	0.7 (57)	0.5 (39)	(5)	(3)
7 Dec 17	102 (8,816)	148 (12,760)	31 (2,707)	40 (3,425)	11 (967)	14 (1,223)	0.7 (64)	0.9 (81)	(4)	(5)
15 Dec 17	—	—	23 (1,990)	13 (1,107)	7 (575)	4 (320)	0.5 (41)	0.3 (23)	(3)	(2)
16 Dec 17	—	—	44 (3,844)	33 (2,839)	17 (1,448)	11 (928)	1.4 (119)	0.9 (76)	(11)	(7)
17 Dec 17	689 (59,571)	458 (39,561)	32 (2,726)	27 (2,296)	7 (562)	4 (340)	0.5 (39)	0.3 (24)	(3)	(2)
19 Dec 17	—	—	20 (1,761)	11 (984)	7 (625)	3 (242)	0.7 (58)	0.3 (22)	(6)	(2)
20 Dec 17	—	—	30 (2,617)	22 (1,881)	9 (771)	5 (471)	0.7 (58)	0.4 (35)	(6)	(4)
(a1) Nevado del Ruiz—Volatile flux estimates derived from SO_2 measurements (dual UV camera system)										
1 Jul 17	—	—	59 (5,076)	41 (3,542)	21 (7)	1,823 (632)	2 (195)	1 (67)	(12)	(4)
4 Jul 17	—	—	72 (6,185)	38 (3,275)	11 (934)	4 (329)	1 (91)	0 (32)	(5)	(2)
(b) Galeras—Volatile flux estimates derived from SO_2 flux daily averages (NOVAC)										
17 Oct 14	38 (3,287)	13 (1,090)	21 (1,784)	7 (591)	5.0 (436)	1.4 (118)	1.5 (126)	0.4 (36)	(0.6)	(0.2)
26 Feb 16	—	—	53 (4,592)	30 (2,573)	5.8 (500)	2.3 (195)	—	—	—	—
29 Feb 16	—	—	67 (5,796)	32 (2,768)	6.4 (550)	2.5 (215)	—	—	—	—
27 Apr 16	—	—	37 (3,229)	15 (1,291)	3.8 (330)	1.5 (129)	—	—	—	—
31 May 16	—	—	35 (3,000)	14 (1,233)	3.5 (300)	1.4 (117)	—	—	—	—
13 Jul 16	—	—	38 (3,256)	18 (1,553)	4.1 (356)	1.6 (138)	—	—	—	—
18 Jul 16	—	—	64 (5,544)	28 (2,393)	8.7 (748)	3.5 (306)	—	—	—	—
21 Mar 17	No plume registered by NOVAC									
13 Jul 17	No plume registered by NOVAC									
14 Jul 17	No plume registered by NOVAC									
(b1) Galeras—Volatile flux estimates derived from SO_2 measurements (dual UV camera system)										
21 Mar 17										
Paisita	50 (4,346)	47 (4,078)	26 (2,249)	25 (2,122)	0.4 (37)	0.4 (35)	0.4 (32)	0.4 (30)	—	—
Chavas	120 (10,340)	55 (4,779)	5 (420)	2 (203)	1.3 (112)	0.6 (52)	1.6 (138)	0.8 (65)	(4.3)	(1.4)
Central crater	—	—	52 (4,456)	29 (2,524)	0.8 (69)	0.5 (39)	1.0 (88)	0.6 (51)	(6.8)	(1.3)
System total	170 (5,991)	103 (8,856)	82 (7,124)	56 (4,844)	2.5 (216)	1.5 (125)	3.0 (259)	1.7 (146)	(11)	(2.7)
(c) Puracé—Volatile flux estimates derived from SO_2 flux daily averages (NOVAC)										
23 Mar 17	4.7 (406)	2.4 (207)	0.9 (84)	0.5 (41)	0.1 (8.8)	0.04 (3.7)	0.02 (2.1)	0.01 (1.1)	(0.09)	(0.05)

Note. Errors are expressed as the standard error of the regression analysis and subsequent error propagation, error on inferred flux propagates error on the SO_2 fluxes and gas ratios. Tables 2a1 (Nevado del Ruiz) and 2b1 (Galeras) show SO_2 flux values acquired using the dual UV camera system. NOVAC = Network for Observation of Volcanic and Atmospheric Change; UV = ultraviolet.

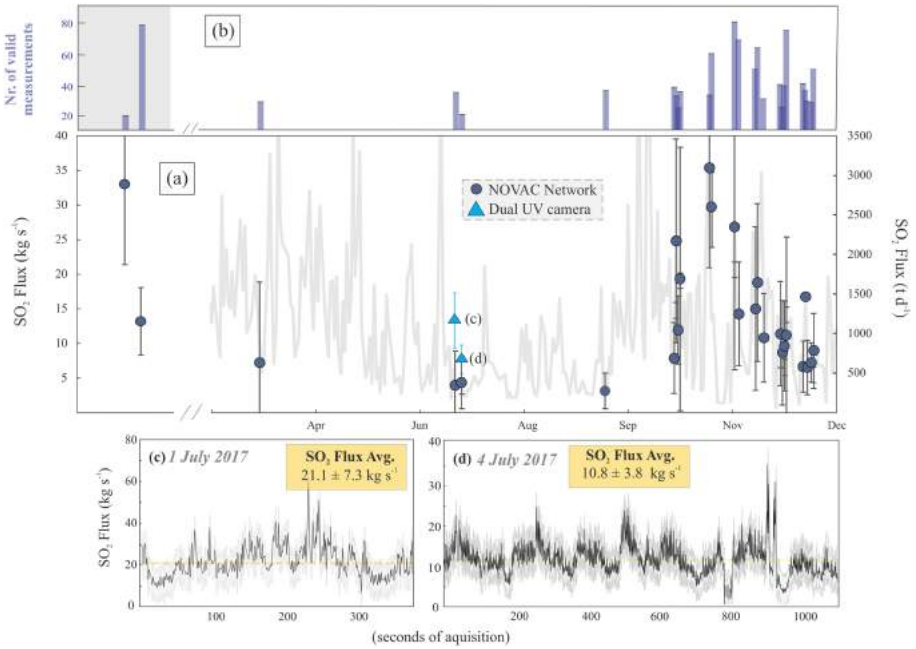

Figure 5. Nevado del Ruiz: (a) SO_2 flux (in kg/s and t/day) time series. Closed circles in dark blue represent daily SO_2 flux means to which blue bars in (b) indicate the number of valid measurements used in each daily average estimate; in (a) March–December (2017) SO_2 flux time series is shown in light gray, and measurements obtained using the dual UV camera system on 1 and 4 July 2017 as blue triangles, with respective acquisition time series (in kg/s) show on (c) 1 and (d) 4 July;. Gray area in (c) and (d) represents the estimated SO_2 flux ± 1σ, with acquisition flux average marked in yellow.

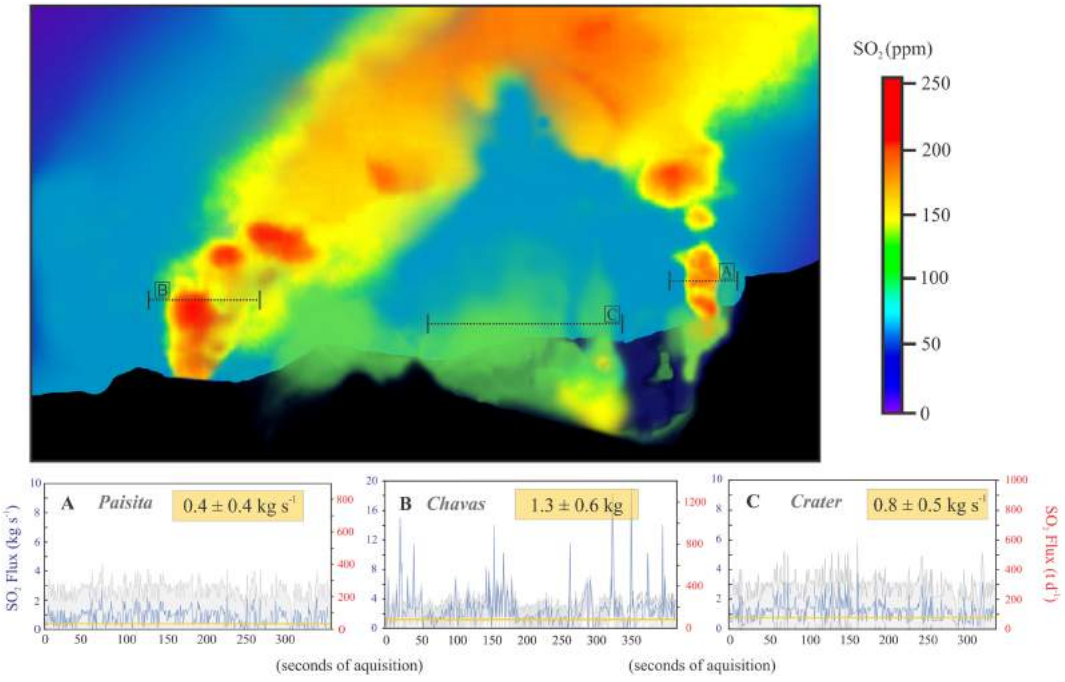

Figure 6. Dual UV camera SO_2 flux retrievals from (a) Paisita, (b) Chavas, and (c) the central crater. Pseudo color image of the fumarolic gas from the three different sources, with dashed line cross sections delimiting the area used to calculate the integrated column amounts of SO_2 using the Vulcamera software (Tamburello, Kantzas, McGonigle, & Aiuppa , 2011). Blue lines in (a)–(c) represent the acquired SO_2 flux time series (± 1σ; in light gray), with acquisition time averages marked in yellow.

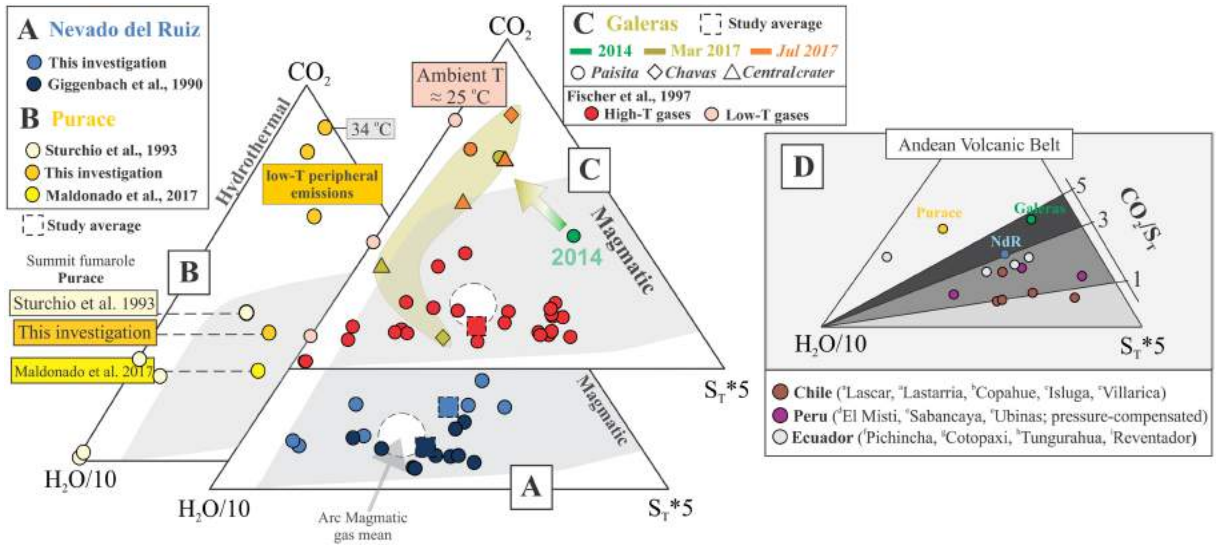

Figure 7. (left) Ternary diagrams showing normalized gas composition for (a) Nevado del Ruiz (in blue), (b) Puracé (in yellow), and (c) Galeras (in red) considering H_2O/10-CO_2-S_T*5 (S_T [SO_2 + H_2S]). Closed circles represent data collected throughout this investigation, whereas square symbols represent reference literature studies for each volcano (Giggenbach et al., 1990 for Nevado del Ruiz; Sturchio et al., 1993 for Puracé; and Fischer et al., 1997 for Galeras). Compositional averages are plotted in dark closed circles (this study) and dark squares (literature). Global magmatic arc-gas samples define the gray area characterized by S-rich gases, with correspondent arc-gas mean estimated by Aiuppa, Fischer, et al. (2017). Red area in (c), plotting along the H_2O-CO_2 axis, marks the compositional shift toward more S-depleted, hydrothermal gases in Galeras from 2014 to 2017. (right) Ternary diagrams showing high-temperature volcanic gas compositions along the Andean Volcanic Belt. Estimated averages from this study are given in triangles, with reference literature averages for Colombia represented in squares. Other arc segments are plotted as follows: (i) In white Ecuador (Guagua Pichincha (Fischer & Chiodini, 2015); Cotopaxi [Hidalgo et al., 2017]; Tungurahua and Reventador (Aiuppa et al., 2019)); (ii) in dark gray Peru (El Misti [Moussallam et al., 2017], Sabancaya and Ubinas [Moussallam, Tamburello, et al., 2017]); and (iii) in light gray Chile (Lascar and Lastarria, (Tamburello et al., 2014); Copahue (Tamburello et al., 2015); Isluga and Tacora (Schipper et al., 2017); Villarica (Aiuppa et al., 2019)). Noticeable trends in CO_2/S_T plotting along the S_T-CO_2 show along-arc trends in volcanic gas compositions for the different segments (yellow graded areas represent, from the bottom, CO_2/S_T = 1, 2, and 5). Note that low-temperature systems such as Guagua Pichincha and Puracé plot near the H_2O-CO_2 axis region due to the S-depleted nature of gas emissions.

and 8). However, according to Giggenbach et al. (1990), the compositions of these low-temperature fumaroles may have been only partially representative of the original magmatic gas signature, owing to potential scrubbing of S (and Cl) during hydrothermal gas-water interactions. Our 2014–2017 plume compositions, in contrast, being fed by high-temperature vent degassing activity from the Arenas crater, are likely more representative of the magmatic conditions at Nevado del Ruiz. The "magmatic" nature of the 2014–2017 plumes is supported by their S-rich compositions (Figure 7a), well within the typical magmatic arc gas range (Aiuppa, Fischer, et al., 2017), and by the prevalence of SO_2 over H_2S (H_2S/SO_2 ratios < 0.2; Figure 8). These SO_2-rich compositions are clear evidence of sustained shallow magma circulation (and degassing) underneath the Arenas crater, as supported by repeated episodes of seismic activity presumably related to active dome emplacement and growth at the summit crater, events closely monitored by the local observatory in Manizales (SGC-OVSM). By averaging our gas data from all categories (I to III), we infer a time-averaged 2014–2017 gas plume composition of 91.7 ± 33.8, 6.0 ± 1.0, and 2.0 ± 1.5 mol% for H_2O, CO_2, and S_T (±1σ). This is only slightly less H_2O rich and more CO_2-S_T rich (e.g., more magmatic in nature) than are the average fumarole compositions of Giggenbach et al. (1990), which reported averages of 95.6, 2.4, and 1.5 mol% for H_2O, CO_2, and S_T, respectively. Both data sets show a similar spread of compositions around the average (see Figure 7a). Chemical variability in the Giggenbach et al. (1990) data set likely reflects variable extents of S scrubbing during hydrothermal processing (and/or meteoric-hydrothermal water addition) in the low-temperature manifestations studied. In contrast, hydrothermal processing is unlikely at the open-vent plume degassing conditions reported here, and the 2014-2017 data scatter are more likely to have been caused by a combination of (i) real temporal variations in degassing dynamics (e.g., variations in melt gas bubble content and gas-melt separation pressure) and/or (ii) the different extents of atmospheric dilution in measured plumes (highlighted by the compositional dependence on $SO_{2\ MAX}$ illustrated in Figures 2 and 3). We argue that the Category I plume data (dilute plume conditions, $SO_{2\ MAX}$ <5), for which more S-poor compositions

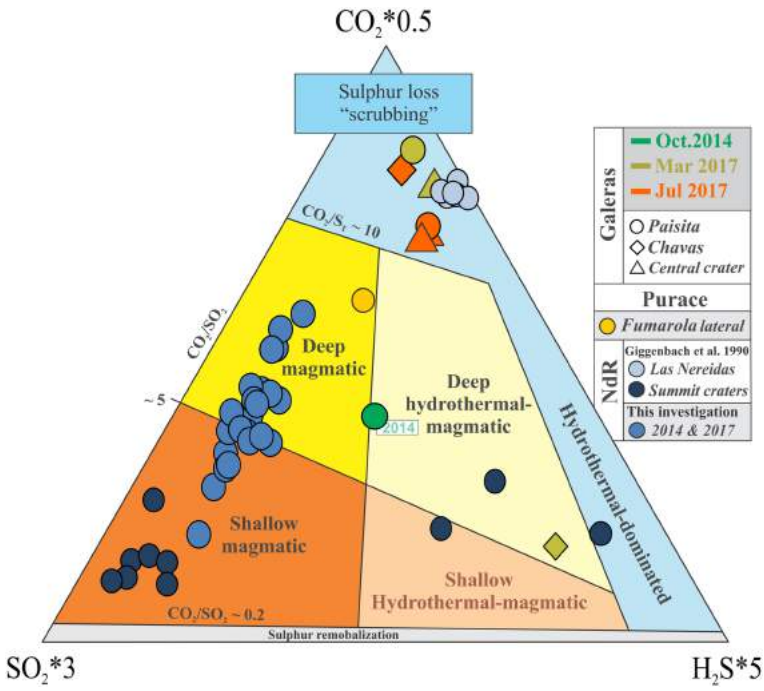

Figure 8. Ternary diagram of SO_2*3-CO_2-H_2S*5 showing hydrothermal-magmatic gas compositions from Nevado del Ruiz (Giggenbach et al., 1990, and this study; in blue), Galeras (2014–2017), and Purace (2017, in yellow). The diagram is adapted from Stix and de Moor (2018). Colored composition fields are based on Aiuppa et al. (2014) and de Moor et al., 2016, 2017. Source boundaries are estimated with key gas ratio values reported for Central American Volcanic Arc volcanism.

(e.g., higher CO_2/S_T and H_2O/S_T) are observed, do likely overestimate the real magmatic signature, due to less accurate corrections of background CO_2 and H_2O contents and/or because of additional gas sources. Therefore, we infer the magmatic CO_2/S_T and H_2O/S_T ratios at 3.9 ± 1.6 and 63 ± 45 by averaging Category II and III data only (Figures 2c, 2d, and 7).

In contrast to the magmatic signature of the Nevado del Ruiz plume(s), measurements taken at both Puracé (Figure 7b) and Galeras (Figure 7c) imply a more hydrothermal nature of the emitted gases. The Puracé gases, in particular, are S depleted relative to the Nevado del Ruiz magmatic field, implying some extent of hydrothermal processing (S scrubbing). Even the hottest of the Puracé fumaroles (*fumarola lateral*, T = 135 °C) has CO_2/S_T ratio of 14.0 ± 2.3, a factor of ~3 higher than in the "magmatic" Nevado del Ruiz gas. Hydrothermal processing in this fumarole is also supported by the higher H_2S/SO_2 (0.7) and H_2/SO_2 (0.3) ratios (the H_2/SO_2 ratio averaged <0.2 at Nevado del Ruiz). Thus, although the presence of SO_2 in the gas confirms some extent of magmatic gas supply to the system (Maldonado et al., 2017), still hydrothermal reactions appear to play a decisive control on the composition of the emitted gases. This is even more so for the low-temperature, CO_2-rich (up to ~90 mol% of CO_2 at San Juan de Puracé) hydrothermal fumaroles located on the volcano's periphery, in which any magmatic SO_2 has been scavenged by percolating meteoric and hydrothermal fluids and eventually converted into H_2S during hydrothermal reactions (Sturchio et al., 1993). Here CO_2/S_T ratios range from ~30 to 55.

Interestingly, our 2014–2017 observations also reveal a hydrothermal gas signature for Galeras, which contrasts with the magmatic (S_T-rich) gas signature reported during intense, high-temperature (up to >600 °C) degassing in the late 1980s to mid-1990s (Fischer et al., 1997; see Figure 7c). In particular, the Galeras gases in 2017, when the most detailed surveys took place, plot close to the H_2O-CO_2 axis (Figure 7c), and their hydrothermal signature is confirmed by a time-averaged composition of 77.4 ± 10.2 mol% H_2O, 21.6 ± 3.0 mol% CO_2, and 0.9 ± 0.1 S_T (here excluding the more "magmatic" composition measured in Chavas in March 2017 of mol% of 97.0 ± 2.4, 1.6 ± 0.2, and 1.0 ± 0.1 for H_2O, CO_2, and S_T, respectively). These are far more S depleted relative to the typical magmatic arc gas signatures reported by Fischer et al. (1997) for

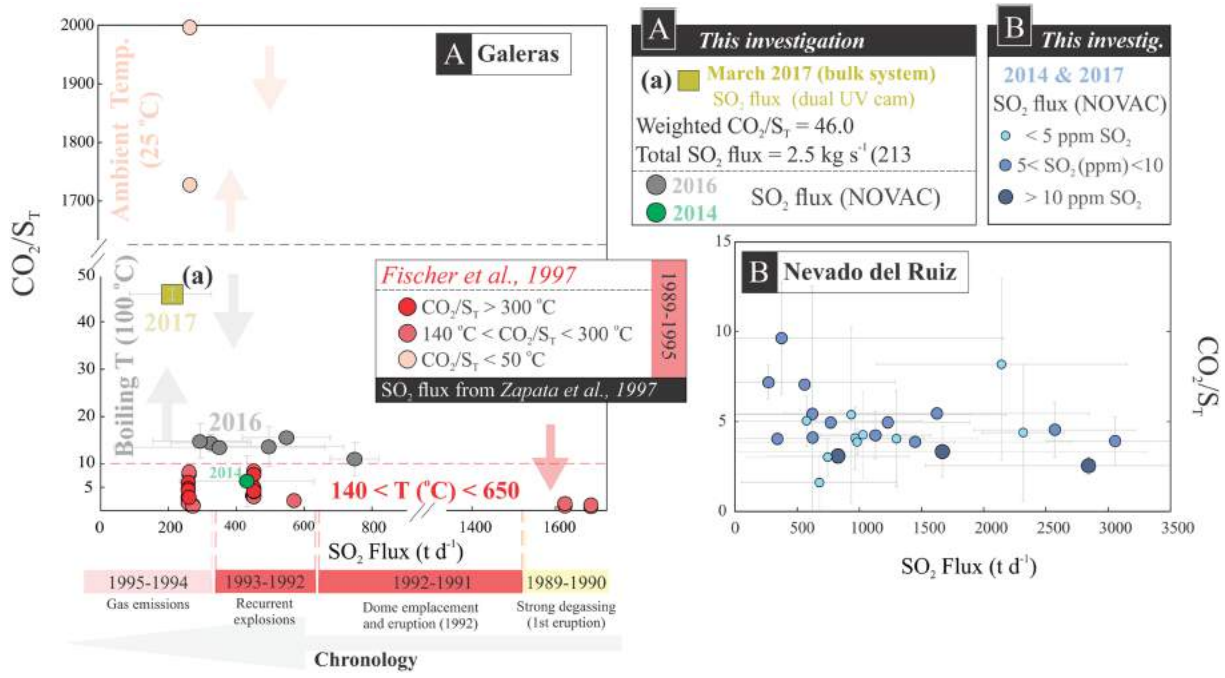

Figure 9. (a) Galeras: CO_2/S_T versus SO_2 flux (t/day) from 1989 to 1995 (CO_2/S_T from Fischer et al., 1997, and SO_2 flux data from Zapata et al., 1997), in different shades of red representing different gas temperature ranges. February–July 2016 data in gray (SO_2 flux records from NOVAC) and 2017 data in olive drab square (SO_2 flux estimates from dual UV camera system); 1989–1995 activity chronology at Galeras is given below (a) (from Zapata et al., 1997). (b) Nevado del Ruiz: CO_2/S_T versus SO_2 flux (t/day), in blue. Categories I to III are distinguishable by different circle sizes, and darker tones of blue for higher SO_2 concentrations.

the 1988–1995 period (mean composition 94.4, 3.6, and 1.9 mol% of H_2O, CO_2, and S_T). The hydrothermal signature of the Galeras gases is also well consistent with the more reducing redox conditions (H_2S/SO_2 and H_2/SO_2 >1; Table 1b) relative to Nevado del Ruiz gas (see also Figure 8, where the majority of the Galeras samples fall within the "hydrothermal-dominated" field determined by Stix & de Moor, 2018, for arc gases from Central American Volcanic Arc).

To better understand the mechanisms controlling the hydrothermal nature of Galeras gases, we integrated our SO_2 flux and CO_2/S_T data (2014–2017) with previous gas information reported for the 1988–1995 period of volcanic unrest at Galeras (Fischer et al., 1997; Zapata et al., 1997; Figure 9a). In its recent history, Galeras has exhibited a wide range of SO_2 fluxes, with emission peaks between 1989 and 1990 (yearly averages of ~19 kg/s, or >1,600 t/day), followed by a general decline between 1991 and 1993 (yearly averages of 3.0–6.6 kg/s, or 260–572 t/day) and then a more sustained drop in the two years that followed (yearly average ~2 kg/s, or ~262 t/day, between 1994 and 1995; Zapata et al., 1997; Figure 9a). Our new results show that between 2014 and 2017, the SO_2 flux has systematically remained <10 kg/s, with the majority of the recorded fluxes ranging between 3 and 6 kg/s (~300 to 500 t/day). This suggests a reduced magmatic gas supply relative to the 1989-1990 degassing unrest, when the CO_2/S_T ratios were consistently (and systematically) the lowest (e.g., more magmatic in nature; Fischer et al., 1997; see Figure 9a). The lowest SO_2 fluxes on our records were measured in 2017, when no reliable SO_2 flux was derived by the NOVAC scanning DOAS, and low fluxes (~2.5 kg/s) were consistently measured by our more proximal UV camera observations (Figure 6). Contemporarily, the highest CO_2/S_T ratios were also measured from fumarolic discharges in Galeras (Figures 4 and 9a). We thus conclude that a reduced magmatic gas transport, combined with a more intense S scrubbing in the shallow hydrothermal system, was the most likely factor governing the observed gas compositional contrast between 2017 and 1989–1990 (Figure 9a). Variable extents of magmatic S scrubbing in the shallow hydrothermal system may also explain the chemical heterogeneities observed between the different Galeras emission sources in 2017 (Paisita, Chavas, and the central crater). Our vent-resolved SO_2 flux observations in March clearly show that most S-depleted gas compositions at Paisita (CO_2/SO_2 ratio of 87.3 ± 17.4) corresponded to the lowest SO_2 fluxes (~0.4 kg/s), while somewhat more magmatic CO_2/SO_2

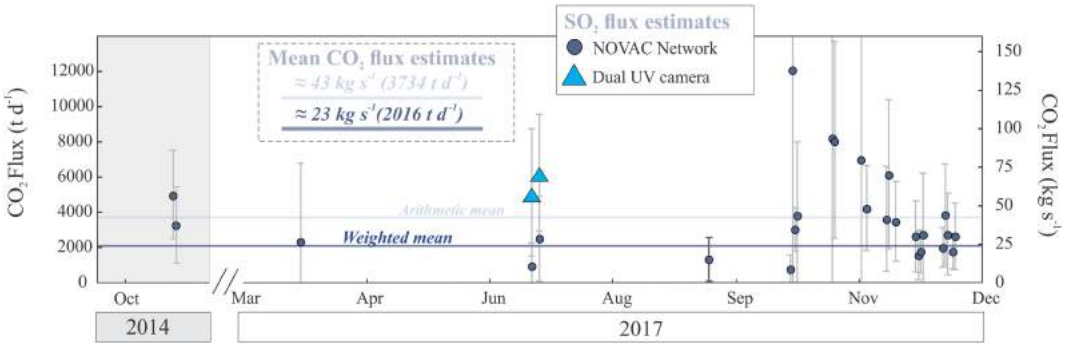

Figure 10. CO_2 time series for Nevado del Ruiz (in kg/s and t/day) for October 2014 and from March to December 2017. Note that CO_2 flux estimates are restricted to days in which volcanic gas compositions were acquired. Weighted mean was calculated using only CO_2 flux measurements whose error is constrained within 100% of the average. Estimates of CO_2 fluxes combining CO_2/SO_2 with the dual UV camera portable system are represented as triangles as a reference, and the arithmetic mean including all estimates is given also as a comparison. Errors (σ) are expressed as the standard error of the regression analysis and subsequent error propagation on the SO_2 fluxes and x/SO_2 ratios.

ratios (5.4 ± 0.8) were simultaneously observed at Chavas, the most actively degassing vent at that time (~1.3 kg/s).

Our 2014–2016 SO_2 fluxes were in the same range as in 1991–1993, yet the gas CO_2/S_T ratios were sizably higher, especially in 2016 (Figure 9a). We ascribe this compositional difference to the significantly different vent temperatures observed in 2014–2016 (fumaroles close to boiling temperatures) and those reported between 1991 and 1993 (140–650 °C). Lower vent temperatures imply more intense S scrubbing along the vent feeding chimneys (Aiuppa, Fischer, et al., 2017), thus contributing to a more hydrothermal gas signature compared to the magmatic (S_T-rich) compositions observed during intense, high-temperature degassing (Fischer et al., 1997; see Figure 7c). Sulfur dioxide fluxes and CO_2/S_T data are also shown for Nevado del Ruiz in Figure 9b.

5.2. Gas Fluxes and Implications for the CAS Volatile Budget

Carbon dioxide and other volatile emissions can be derived for each of the three volcanoes by combining the coacquired SO_2 fluxes (Table 2) and volcanic gas CO_2/SO_2 ratios (Table 1). The uncertainties reported in this section are expressed as the standard error of the regression analysis and subsequent error propagation; error on inferred flux propagates error on the SO_2 fluxes and x/SO_2 ratios.

At Nevado del Ruiz, we establish a CO_2 flux time series (Figure 10) by using in tandem, for each measurement day, the daily averaged CO_2/SO_2 ratios (Figure 3) and SO_2 flux estimates (Figure 5). The so derived daily averaged CO_2 fluxes range from ~9 to 139 kg/s (arithmetic mean, 43 ± 30) and have associated errors of 40% to >100%. These large uncertainties reflect the large interdaily variability of both CO_2/SO_2 ratios and, especially, that of SO_2 fluxes, possibly caused by (i) the nonstationary nature of degassing at Nevado del Ruiz that consists of intermittent large pulses of SO_2 release interspersed within phases of milder and more continuous SO_2 degassing (e.g., Dinger et al., 2018; Malinconico, 1987), and (ii) the complex wind field patterns at the volcano's height that produce erratic changes in plume transport direction and speed (these being hard to quantify and taken into account in flux calculations). Here we attempted to minimize the effect of a time-variable atmospheric plume dispersion, by applying a set of filtering parameters (see supporting information Text S1) that only scans the captured ≥85% of the gas plume that were selected for daily average estimates. Still, the daily variability of our NOVAC-based SO_2 fluxes remain large (39% and above).

In view of the above, we find it more prudent to derive the long-term SO_2 and CO_2 emission budgets for Nevado del Ruiz by deriving weighted flux averages based on the standard deviations of each daily measurement (Figures 5 and 10). Doing so, the daily gas fluxes with lower variability are assigned a proportionally higher weight in the mean flux calculation (note that for CO_2, the daily averaged fluxes with >100% relative uncertainty are not used in the calculation). From this method, we derive a time-averaged SO_2 flux weighted mean of ~8 kg/s, well below the arithmetic mean flux of 14 kg/s and at the lower range of the daily SO_2 fluxes

Table 3
Weighted TV Flux Averages for Nevado del Ruiz, Galeras, and Puracé

Volcano	H_2O in kg/s (t/day)	CO_2 in kg/s (t/day)	SO_2 in kg/s (t/day)	H_2S in kg/s (t/day)	H_2 in kg/s (t/day)	TV flux in kg/s (t/day)
Nevado del Ruiz	157 (13,586)	23 (2,017)	7.8 (672)	0.6 (52)	(3.4)	189 (16,330)
Galeras	40 (3,457)	30 (2,600)	4.2 (365)	1.4 (119)	(0.7)	76 (6,543)
Puracé	4.7 (406)	1.0 (84)	0.1 (8.8)	0.02 (2.1)	(0.09)	5.8 (502)

Note. Averages are calculated based on daily uncertainties of both composition (x/SO_2; daily uncertainties reported in Tables 1a–1c) and SO_2 flux measurements (daily uncertainties reported in Tables 2a–2c). TV flux = total volatile flux.

reported (~$3_{[min]}$–$35_{[max]}$ kg/s; Table 2). Similarly, we estimate a weighted CO_2 flux average of ~23 kg/s, which is ~50% lower than the arithmetic mean (~43 kg/s). The same procedure leads to deriving H_2O, H_2S, and H_2 fluxes of ~330, 0.6, and 0.05 kg/s, from which we infer a time-averaged total volatile flux (TV flux) for Nevado del Ruiz in 2014–2017 of ~363 kg/s (~31,300 t/day). In comparison with other persistently active arc sources, for example, Aiuppa et al. (2008) estimated a TV flux for Mount Etna of ~243 kg/s (or ~21,000 t/day), while Bani et al. (2018) reported TV flux estimates of ~172 kg/s for Dukono. Despite the big uncertainties associated with studies of this nature, such comparisons do provide strong evidence that Nevado del Ruiz is, in fact, one of the strongest volcanic arc gas point sources globally.

Within the CAS, Galeras and Puracé volatile budgets are here characterized, although with a lower level of detail (Tables 2b and 2c, respectively). At Puracé, we only have compositional data for one measurement day (23 March 2017; Table 1c). By scaling this by the NOVAC-based daily averaged SO_2 flux of ~0.1 kg/s (or 9 ± 4 t/day), we assess the H_2O and CO_2 fluxes at 6 ± 1 and 1 ± 0.2 kg/s respectively. The TV flux from summit subaerial discharges (*fumarola lateral*) is thus estimated at 7 kg/s (or 600 t/day TV flux), to which both H_2S and H_2 contribute $\ll$0.1 kg/s. This is a factor ~10 less than the TV flux reported by Maldonado et al. (2017) of 73 kg/s (or ~6340 t/day) derived in 2016, who yet used a much higher SO_2 flux of ~2 kg/s (208 t/day). Clearly, the volatile emissions from Puracé are not stationary over time, and simultaneous composition and flux records are required.

At Galeras, both compositions and fluxes have repeatedly been measured in 2014–2017. The majority of the SO_2 flux records are from the scanning NOVAC instrument and are thus representative of the bulk plume. Between 2014 and 2016 our compositional measurements focused on the Paisita summit fumarole (cf. section 3), whose vigorous degassing clearly prevailed over any other summit fumarolic volatile discharge over that period. Our 2014–2016 volatile flux estimates (Table 2) are thus based on the assumption that the Paisita fumarole was representative of the bulk plume composition. In 2017 a large vent-to-vent chemical variability was observed, and thus, the volatile fluxes for Paisita, Chavas, and the central crater are independently evaluated (Table 2) using the vent-resolved SO_2 flux results obtained with the UV camera on 21 March 2017 (Figure 6). From these, and from the coacquired compositional data (Table 1), the weighted bulk volatile flux average (2014–2017) for Galeras is estimated at ~76 kg/s (or ~6,543-t/day TV flux; Table 3). It is important to note that our average estimates (Table 3) are weighted based on the daily uncertainties of gas composition (x/SO_2) and SO_2 fluxes reported for each day. Therefore, we here report a TV flux that is unsurprisingly much closer to the values reported in 2014 than to those of 2017, as a result of more favorable measurement conditions (especially in situ composition measurements favored by less diluted gas plumes) due to the system's more persistent degassing (see section 4.2) at the beginning of this study. According to our calculations, a recent (2014–2017) time-averaged CO_2 output from Galeras of ~30 kg/s, more than a factor of 2 larger than the 1989–1995 time-averaged CO_2 output of 12 kg/s (Zapata et al., 1997) clearly indicates that the volcano remains a significant volcanic CO_2 source even during the ongoing period of quiescence and hydrothermal degassing (Figure 11).

The cumulative CO_2 flux contribution from Nevado del Ruiz, Galeras, and Puracé is thus estimated at ~54 kg/s (or ~4,701 t/day; Figure 11). Nevado del Huila (e.g. Pulgarín et al., 2001), another relevant subaerial emission source in the CAS, has been persistently degassing over the last decades, especially during its most recent eruptive period (2009–2012) when it emitted ~862 t/day of CO_2 (Aiuppa et al., 2019). We here use these estimations to infer a total volcanic CO_2 flux from the four most actively degassing CAS subaerial volcanoes at approximately 5,563 t/day. In perspective, this corresponds to more than 50% of present-day (2005–2015) total volcanic CO_2 emissions from the active volcanoes of the Andean Volcanic Belt (derived at

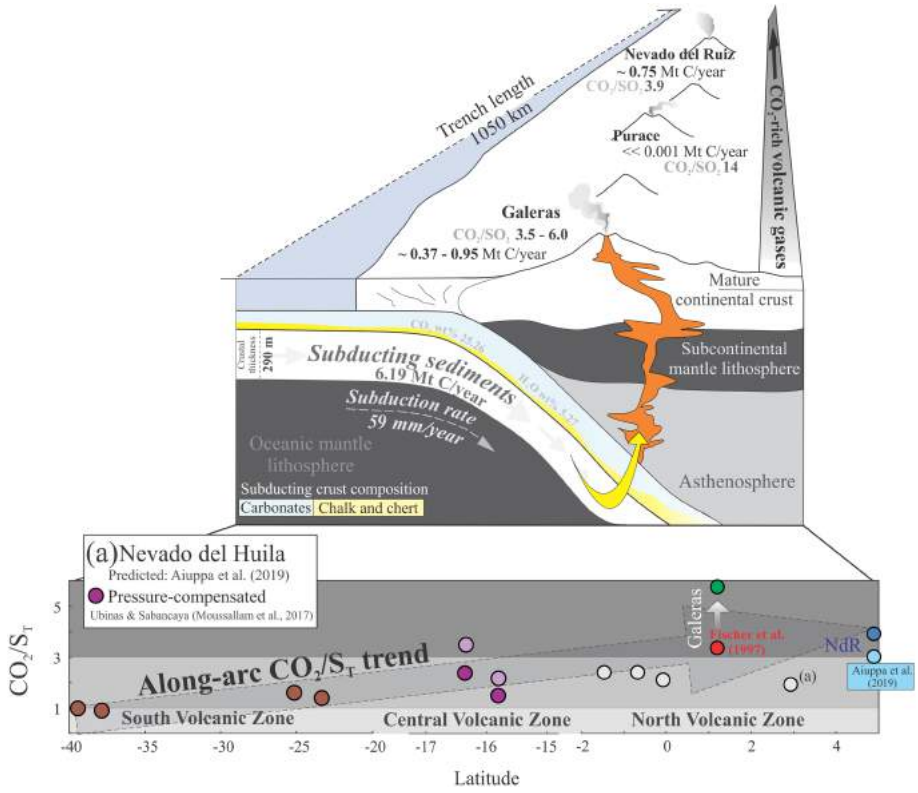

Figure 11. Schematic figure showing the nature of the sediments subducting underneath the Colombian Arc Segment (CAS), with respective sediment composition. Estimated carbon fluxes (in Mt C/year) and gas compositions estimated in here are given for Nevado del Ruiz, Puracé, and Galeras. The quoted CO_2 output range for Galeras is based upon a combination of 2014–2017 (this study) and 1989–1995 (Zapata et al., 1997) results. The bottom plot illustrates the along-arc variations in gas CO_2/S_T ratio signature in South America. For Galeras, we report the more magmatic-in-nature CO_2/S_T ratio (green circle; October 2014) obtained throughout this investigation and compare it with the composition of high-temperature gases collected during the 1989–1995 period of unrest (red circle; Fischer et al., 1997; Aiuppa, Fischer, et al., 2017). For Nevado del Ruiz, the original CO_2/S_T ratio quoted in Aiuppa et al. (2019) is shown for comparison. Both pressure-compensated and uncorrected CO_2/S_T for Sabancaya and Ubinas (Peru; Moussallam, Tamburello, et al., 2017) are given for comparison.

~10,000 t/day from data in Aiuppa et al., 2019). Notably, Nevado del Ruiz and Galeras together contribute ~35% to the subaerial volcanic CO_2 emission budget in the Andean Volcanic Belt and are thus larger CO_2 sources than any other active volcano in Ecuador (Hidalgo et al., 2016, 2018), Peru (Moussallam et al., 2017; Moussallam, Tamburello, et al., 2017), and Chile (Tamburello et al., 2014).

5.3. Along-Trench CO_2/S_T Variations and Volatile Recycling

Our results above provide novel information on the geochemical cycle of C, and other volatiles, through subduction zones (e.g., the fraction of slab-derived C being recycled through subaerial degassing along the CAS). Plank and Langmuir (1988) first investigated the chemical nature of the sediments subducting underneath the Colombian trench and reported approximately 50% carbonate in the bulk core. A recent update by Plank (2014) on bulk concentration data for this arc segment confirms the C-rich nature of these sediments (predominantly siliceous oozes and limestones), with CO_2 and H_2O bulk sediment concentrations of 25.26 and 5.27 (wt%), respectively. From this, we estimate that about 6.19×10^{12} g C/year are being subducted through slab sediments underneath the CAS (von Huene & Scholl, 1991; Jarrard, 2003; Syracuse & Abers, 2006; see supporting information Text S2 for details on the calculations).

However, other C sources (e.g., sedimentary organic C) may play a significant role in the remobilization of C, and such contributions can be distinguished based on observed $CO_2/^3He$ ratios and $\delta^{13}C$ isotopic signatures (Sano & Marty, 1995). To the best of our knowledge, $\delta^{13}C$ isotope characterization of Nevado del Ruiz has

only been reported for thermal and surface waters related to the hydrothermal system of the volcano (Sturchio et al., 1988). These low-temperature media (below boiling) show isotopic signatures as light as −11.4‰, which likely reflect various extents of isotope fractionation and/or mixing of magmatic and organic components. At Pandiaco mineral spring (Galeras) low-temperature gas discharges (consisting of almost pure CO_2; see Sano et al., 1997) also yield isotopic signatures more organic in nature ($\delta^{13}C$ values as negative as −9.16‰) with negligibly small mantle Carbon contribution. For temperature ranges similar to those of Nevado del Ruiz thermal waters and Pandiaco (Galeras), Purace also show $\delta^{13}C$ isotopic values as low as −11.5‰ (Sturchio et al., 1988). Although this data has proved crucial to our understanding of hydrothermal systems, it is most likely not representative of the magmatic end-member of these volcanic systems. On the other hand, high-temperature crater samples (up to 350 °C) reported by Sano et al. (1997) for Galeras consistently fall within mid-ocean ridge basalt range (5‰ ± 3‰). In addition, high-temperature fumarole data consistently displaying $CO_2/^3He$ ratios (average 2.3×10^{10} from Sano & Williams, 1996, and Sano et al., 1997) 1 order of magnitude greater than the mid-ocean ridge basalt range ($2 \pm 1 \times 10^9$; see Marty & Tolstikhin, 1998) possibly reveal the addition of slab-derived carbon to the mantle component. The same authors attribute up to 79% of the C to be derived from limestone (including slab carbonate), which suggests that slab-derived C represents indeed a very considerable portion of total C in the system. Moreover, unusually high (for arc volcanoes) $^3He/^4He$ ratios reported for high-temperature gas emissions (350 °C) in Galeras (as high as 8.8 Ra; see Sano et al., 1997) also suggest a minor role of the crustal component in the Galeras gas emissions.

Therefore, based on our estimates in section 5.2, we infer that subaerial degassing volcanoes along the CAS are currently releasing a small fraction (roughly 30%, or 2.0×10^{12} g C/year) of the carbon being subducted in this region. This mismatch between C inputs at trench and C outputs at the Colombian trench is most likely larger if considering other C sources, as discussed above. However, our reports contribute additional information to earlier calculations made for other arc segments (e.g., de Moor et al., 2017; Hilton et al., 2002) and implies (i) a limited C recycling efficiency in the slab (due to high slab carbonate stability (see recent discussion by Keleman &Manning, 2013); (ii) that C is primarily recycled by forms of degassing other than plumes/fumaroles at central volcanoes (e.g., soils and/or groundwater; Chiodini et al., 1998; Tamburello et al., 2018); or (iii) that significant carbon sequestration occurs in the forearc crust, as suggested by Barry et al. (2019).

The data set of Plank (2013) also identifies substantial along-arc variations in the mineralogy and chemistry of sediments subducting underneath the Andean Volcanic Belt. In particular, it is shown that the CO_2 content of the subducting sediments decreases southward along the arc, from 25.26 wt% in the NVZ (Colombia), 24.53 wt% in the CVZ (Peru), to 0–1.5 wt% in the Chilean segment of the arc (Figure 10). Our novel gas compositional data for Nevado de Ruiz, combined with available magmatic gas information for Galeras (Fischer et al., 1997), and other strongly degassing volcanoes in the Andes (see legend of Figure 7 for data provenance), allow us to more fully characterize the along-arc variations in the gas CO_2/S_T ratio, as illustrated in Figure 11. Interestingly, we find a systematic along-arc trend in the magmatic gas CO_2/S_T ratio, which decreases from ~5 in Colombia, ~2 in the CVZ (Moussallam et al., 2017; Moussallam, Tamburello, et al., 2017), to ~1 in southern Chile (Tamburello et al., 2015), thus matching the north-to-south decrease in the sediment CO_2 contents, described above. This observation provides additional experimental evidence for earlier indications from a global data set (Aiuppa, Fischer, et al., 2017; Aiuppa et al., 2019) that slab sediment composition plays a decisive control on the CO_2/S_T ratio signature of arc magmatic gases. We ultimately propose that although the C recycling efficiency along the CAS is likely to be low (see above), sediments subducted at the Colombian trench are so C enriched to impart a high CO_2/S_T ratio signature to the magmatic gases degassed in the overlying volcanic arc.

6. Conclusions

We reported on the composition and flux of gases emitted along the CAS of the NVZ between 2014 and 2017, measuring in situ volcanic gas compositions using a MultiGAS and estimating SO_2 fluxes by using scanning UV spectrometers and UV cameras. Despite the wide range in gas composition and flux values observed, mostly due to variables associated with degassing dynamics and measurement difficulties at such extreme conditions, data here reported stress the importance of the ongoing efforts to quantify subaerial volatile (especially CO_2) emissions from arc volcanism. This study shows that Nevado del Ruiz and Galeras

together contribute about 20% to the total subaerial CO_2 emissions of the volcanic arc (~2,017 t/day), clearly reinforcing the importance of newly reported data in the context of global arc volatile emissions. Furthermore, combining this with our updated estimates of subaerial CO_2 emissions rates for Puracé (84 t/day) and the current estimates of ~860 t/day for Nevado del Huila, our work shows that this segment of the arc is responsible for one third of the total subaerial CO_2 of the entire Andean trench, when accounting for the strongest, most persistently degassing volcanoes along the arc. We therefore suggest a strong correlation between subducted sediment compositions at this segment (25.26 CO_2 wt%; 1.50 CO_2 wt% at SVZ in comparison) with here highlighted CO_2/S_T northward increase (Nevado del Ruiz and Galeras ~4–6), once again validating the study of volcanic gas chemistry and arc-scale trends in volatile composition as a powerful tool to investigate processes of volatile input and recycling into the mantle wedge via the subducted slab. We estimate that about one third (~2 Mt C/year) of the C being subducted (~6.19 Mt C/year) gets resurfaced through subaerial volcanic gas emissions in Colombia (NdR ~0.7 Mt C/year). Finally, newly established temporally resolved volcanic gas time series for Nevado del Ruiz and Galeras set a crucial background in gas-related monitoring parameters (e.g., CO_2/SO_2, proven to be a powerful monitoring tool especially for CO_2-rich volcanic systems) and will hopefully help the ongoing efforts to predict transitions from quiescence to periods of volcanic unrest at such hazardous volcanoes.

Acknowledgments
We are deeply grateful to all the *Servicio Geológico Colombiano* staff and *Observatorios Vulcanológicos y Sismológicos* of Manizales, Popayán, and Pasto personnel for their continuous logistical and scientific support throughout this investigation. Initial funding for producing the NOVAC data set here presented was provided by the European Commission FP5 (DORSIVA project) and FP6 (NOVAC project), and the operation of the NOVAC network is funded through initiatives of the Volcano Observatories and support from the Volcano Disaster Assistance Program of the United States Geological Survey (SGS). We would also like to acknowledge the crucial support from the Alfred P. Sloan Foundation (Deep Carbon Observatory/DECADE project; UniPa-CiW subcontract 10881-1262) and the MIUR (under grant PRIN2017-2017LMNLAW) for funding a large portion of this project. This manuscript has benefited from constructive reviews from Felipe Aguilera, Maarten de Moor, and one anonymous reviewer. The new data set generated in this study is available at the EarthChem data repository (https://doi.org/10.1594/IEDA/111393).

References

Aiuppa, A., Bitetto, M., Francofonte, V., Velasquez, G., Parra, C. B., Giudice, G., et al. (2017). A CO_2-gas precursor to the March 2015 Villarrica volcano eruption. *Geochemistry, Geophysics, Geosystems*, *18*, 2120–2132. https://doi.org/10.1002/2017GC006892

Aiuppa, A., Federico, C., Giudice, G., Gurrieri, S., Liuzzo, M., Shinohara, H., et al. (2006). Rates of carbon dioxide plume degassing from Mount Etna volcano. *Journal of Geophysical Research*, *111*, B09207. https://doi.org/10.1029/2006JB004307

Aiuppa, A., Fiorani, L., Santoro, S., Parracino, S., Nuvoli, M., Chiodini, G., et al. (2015). New ground-based LIDAR enables volcanic CO_2 flux measurements. *Scientific Reports*, *5*. https://doi.org/10.1038/srep13614

Aiuppa, A., Fischer, T. P., Plank, T., & Bani, P. (2019). CO_2 flux emissions from the Earth's most actively degassing volcanoes, 2005–2015. *Scientific Reports*, *9*(5442). https://doi.org/10.1038/s41598-019-41901-y

Aiuppa, A., Fischer, T. P., Plank, T., Robidoux, P., & Di Napoli, R. (2017). Along-arc and inter-arc variations in volcanic gas CO_2/S_T ratios reveal dual source of carbon in arc volcanism. *Earth-Science Reviews*, *168*, 24–47. https://doi.org/10.1016/j.earscirev.2017.03.005

Aiuppa, A., Frederico, C., Guidice, G., & Gurrieri, S. (2005). Chemical mapping of a fumarolic field: La Fossa Crater, Vulcano Island (Aeolian Islands, Italy). *Geophysical Research Letters*, *32*, L13309. https://doi.org/10.1029/2005GL023207

Aiuppa, A., Giudice, G., Gurrieri, S., Liuzzo, M., Burton, M., Caltabiano, T., et al. (2008). Total volatile flux from Mount Etna. *Geophysical Research Letters*, *35*, L24302. https://doi.org/10.1029/2008GL035871

Aiuppa, A., Robidoux, P., Tamburello, G., Conde, V., Galle, B., Avard, G., et al. (2014). Gas measurements from the Costa Rica–Nicaragua volcanic segment suggest possible along-arc variations in volcanic gas chemistry. *Earth and Planetary Science Letters*, *407*, 134–147. https://doi.org/10.1016/j.epsl.2014.09.041

Andres, R. J., & Kasgnoc, A. D. (1998). A time-averaged inventory of subaerial volcanic sulfur emissions. *Journal of Geophysical Research*, *103*, 25251–25261. https://doi.org/10.1029/98JD02091

Arango, E. E., Buitrago, A. J., Cataldi, R., Ferrara, G. C., Panichi, C., & Villegas, V. J. (1970). Preliminary study on the Ruiz Geothermal Project (Colombia). *Geothermics*, *2*, 43–56. https://doi.org/10.1016/0375-6505(70)90005-2

Bani, P., Tamburello, G., Rose-Koga, E. F., Liuzzo, M., Aiuppa, A., Cluzel, N., et al. (2018). Dukono, the predominant source of volcanic degassing in Indonesia, sustained by a depleted Indian-MORB. *Bulletin of Volcanology*, *80*(1). https://doi.org/10.1007/s00445-017-1178-9

Barry, P. H., de Moor, J. M., Giovannelli, D., Schrenk, M., Hummer, D. R., Lopez, T., et al. (2019). Forearc carbon sink reduces long-term volatile recycling into the mantle. *Nature*, *568*, 487–492. https://doi.org/10.1038/s41586-019-1131-5

Boletines Informativos de actividad volcánica, Servicio Geológico Colombiano—Portal Servicio Geológico Colombiano [https://www2.sgc.gov.co/Noticias/Paginas/Boletines.aspx]

Burton, M., & Sawyer, G. (2013). Deep carbon emissions from volcanoes. *Reviews in Mineralogy and Geochemistry*, *75*, 323–354. https://doi.org/10.2138/rmg.2013.75.11

Calvache, M. L. (1990). Geology and volcanology of the recent evolution of Galeras volcano, Colombia. M. S Thesis, Louisiana State University.

Calvache, M. L., Cortes, G. P. J., & Williams, S. N. (1997). Stratigraphy and chronology of the Galeras volcanic complex, Colombia. *Journal of Volcanology and Geothermal Research*, *77*, 5–19. https://doi.org/10.1016/S0377-0273(96)00083-2

Calvache, M. L., & Williams, S. N. (1997a). Emplacement and petrological evolution of the andesitic dome of Galeras volcano, 1990–1992. *Journal of Volcanology and Geothermal Research*, *77*, 57–69. https://doi.org/10.1016/S0377-0273(96)00086-8

Calvache, M. L., & Williams, S. N. (1997b). Geochemistry and petrology of the Galeras Volcanic Complex, Colombia. *Journal of Volcanology and Geothermal Research*, *77*, 21–38. https://doi.org/10.1016/S0377-0273(96)00084-4

Carn, S. A., Fioletov, V. E., McLinden, C. A., Li, C., & Krotkov, N. A. (2017). A decade of global volcanic SO_2 emissions measured from space. *Scientific Reports*, *7*, 44095. https://doi.org/10.1038/srep44095

Chiodini, G., Cionib, R., Guidib, M., Raco, B., & Marinic, L. (1998). Soil CO_2 flux measurements in volcanic and geothermal areas. *Applied Geochemistry*, *13*, 543–552. https://doi.org/10.1016/S0883-2927(97)00076-0

Dasgupta, R. (2013). Ingassing, storage, and outgassing of terrestrial carbon through geologic time. *Reviews in Mineralogy and Geochemistry*, *75*, 183–229. https://doi.org/10.2138/rmg.2013.75.7

de Moor, J. M., Aiuppa, A., Avard, G., Wehrmann, H., Dunbar, N., Muller, C., et al. (2016). Turmoil at Turrialba volcano (Costa Rica): Degassing and eruptive processes inferred from high-frequency gas monitoring. *Journal of Geophysical Research: Solid Earth*, *121*, 5761–5775. https://doi.org/10.1002/2016JB013150

de Moor, J. M., Kern, C., Avard, G., Muller, C., Aiuppa, A., Saballos, A., et al. (2017). A new sulfur and carbon degassing inventory for the Southern Central American Volcanic Arc: The importance of accurate time series datasets and implications for global volatile budgets. *Geochemistry, Geophysics, Geosystems*, *18*, 4437–4468. https://doi.org/10.1002/2017GC007141

Dee, D. P., Uppala, S. M., Simmons, A. J., Berrisford, P., Poli, P., Kobayashi, S., et al. (2011). The ERA-Interim reanalysis: Configuration and performance of the data assimilation system. *Quarterly Journal of the Royal Meteorological Society*, *137*, 553–597. https://doi.org/10.1002/qj.828

Dinger, F., Bobrowski, N., Simon, W., Bredemeyer, S., Hidalgo, S., Arellano, S., et al. (2018). Periodicity in the $BrOSO_2$ molar ratios in the volcanic gas plume of Cotopaxi and its correlation with the Earth tides during the eruption in 2015. *Solid Earth*, *9*, 247–266. https://doi.org/10.5194/se-9-247-2018

Edmonds, M., Herd, R., Galle, B., & Oppenheimer, C. (2003). Automated, high time-resolution measurements of SO_2 flux at Soufrière Hills Volcano, Montserrat. *Bulletin of Volcanology*, *65*, 578–586. https://doi.org/10.1007/s00445-003-0286-x

Fischer, T. P. (2008). Fluxes of volatiles (H_2O, CO_2, N_2, Cl, F) from arc volcanoes. *Geochemical Journal*, *42*, 21–38. https://doi.org/10.2343/geochemj.42.21

Fischer, T. P., & Chiodini, G. (2015). Volcanic, magmatic and hydrothermal gases. *The Encyclopedia of Volcanoes*, *2*, 779–796. https://doi.org/10.1016/B978-0-12-385938-9.00045-6

Fischer, T. P., Sturchio, N. C., Stix, J., Arehart, G. B., Counce, D., & Williams, S. N. (1997). Chemical and isotopic composition of fumarolic gases and spring discharges from Galeras volcano, Colombia. *Journal of Volcanology and Geothermal Research*, *77*, 229–253. https://doi.org/10.1016/S0377-0273(96)00096-0

Galle, B., Johansson, M., Rivera, C., Zhang, Y., Kihlman, M., Kern, C., et al. (2010). Network for Observation of Volcanic and Atmospheric Change (NOVAC)—A global network for volcanic gas monitoring: Network layout and instrument description. *Journal of Geophysical Research*, *115*, D05304. https://doi.org/10.1029/2009JD011823

Galle, B., Oppenheimer, C., Geyer, A., McGonigle, A., Edmonds, M., & Horrocks, L. (2003). A miniaturized ultraviolet spectrometer for remote sensing of SO_2 fluxes: A new tool for volcano surveillance. *Journal of Volcanology and Geothermal Research*, *119*, 241–254. https://doi.org/10.1016/S0377-0273(02)00356-6

Giggenbach, W. F., Garcia, N. P., Londoño, A. C., Rodriguez, L. V., Rojas, N. G., & Calvache, M. L. (1990). The chemistry of fumarolic vapor and thermal-spring discharges from the Nevado del Ruiz volcanic-magmatic-hydrothermal system, Colombia. *Journal of Volcanology and Geothermal Research*, *42*, 13–39. https://doi.org/10.1016/0377-0273(90)90067-P

Global Volcanism Program (2013a). Galeras (351080) in Volcanoes of the world, v. 4.7.7. Venzke, E (ed.). Smithsonian Institution. Downloaded 20 Dec 2018 (https://volcano.si.edu/volcano.cfm?vn=351080). https://doi.org/10.5479/siGVPVOTW42013

Global Volcanism Program (2013b). Nevado del Ruiz (351020) in Volcanoes of the world, v. 4.7.7. Venzke, E (ed.). Smithsonian Institution. Downloaded 20 Dec 2018 (https://volcano.si.edu/volcano.cfm?vn=351020). https://doi.org/10.5479/siGVPVOTW42013

Global Volcanism Program (2013c). Puracé (351060) in Volcanoes of the world, v. 4.7.7. Venzke, E (ed.). Smithsonian Institution. Downloaded 20 Dec 2018 (https://volcano.si.edu/volcano.cfm?vn=351060). https://doi.org/10.5479/siGVPVOTW42013

Hall, M. L. (1990). Chronology of the principal scientific and governmental actions leading up to the November 13, 1985 eruption of Nevado del Ruiz, Colombia. *Journal of Volcanology and Geothermal Research*, *42*, 101–115. https://doi.org/10.1016/0377-0273(90)90072-N

Hidalgo, S., Battaglia, J., Arellano, S., Sierra, D., Bernard, B., Rene, P., et al. (2018). Evolution of the 2015 Cotopaxi eruption revealed by combined geochemical and seismic observations. *Geochemistry, Geophysics, Geosystems*, *19*, 2087–2108. https://doi.org/10.1029/2018GC007514

Hidalgo, S., Battaglia, J., Arellano, S., Sierra, D., Parra, R., Kelly, P., et al. (2016). Geochemical signals of unrest and eruption of Cotopaxi volcano in 2015 (conference paper). *Cities on Volcanoes*, *9*.

Hilton, D. R., Fischer, T. P., & Marty, B. (2002). Noble gases and volatile recycling at subduction zones. *Reviews in Mineralogy and Geochemistry*, *47*(1), 319–370. https://doi.org/10.2138/rmg.2002.47.9

Jarrard, R. D. (1986). Relations among subduction parameters. *Reviews of Geophysics*, *24*, 217–284. https://doi.org/10.1029/RG024i002p00217

Jarrard, R. D. (2003). Subduction fluxes of water, carbon dioxide, chlorine, and potassium. *Geochemistry, Geophysics, Geosystems*, *4*(5), 8905. https://doi.org/10.1029/2002GC000392

Johansson, M., Galle, B., Zhang, Y., Rivera, C., Deliang, C., & Wyser, K. (2009). The dual-beam mini-DOAS technique—Measurements of volcanic gas emission, plume height and plume speed with a single instrument. *Bulletin of Volcanology*, *71*, 747–751. https://doi.org/10.1007/s00445-008-0260-8

Kantzas, E. P., & McGonigle, A. J. S. (2008). Ground based ultraviolet remote sensing of volcanic gas plumes. *Sensors*, *8*. https://doi.org/10.3390/s8031559

Kantzas, E. P., McGonigle, A. J. S., Tamburello, G., Aiuppa, A., & Bryant, R. G. (2010). Protocols for UV camera volcanic SO_2 measurements. *Journal of Volcanology and Geothermal Research*, *194*(1-3), 55–60. https://doi.org/10.1016/j.jvolgeores.2010.05.003

Kelemen, P. B., & Manning, C. E. (2015). Reevaluating carbon fluxes in subduction zones, what goes down, mostly comes up. *PNAS*, *112*(30), 3997–4006. https://doi.org/10.1073/pnas.1507889112

Kern, C., Werner, C., Elias, T., Sutton, A., & Lubcke, P. (2013). Applying UV cameras for SO_2 detection to distant or optically thick volcanic plumes. *Journal of Volcanology and Geothermal Research*, *262*, 80–89. https://doi.org/10.1016/j.jvolgeores.2013.06.009

Lübcke, P., Bobrowski, N., Illing, S., Kern, C., Nieves, J. M. A., Vogel, L., et al. (2012). On the absolute calibration of SO_2 cameras. *Atmospheric Measurement Techniques*, *6*, 677–696. https://doi.org/10.5194/amt-6-677-2013

Maldonado, L. F. M., Inguaggiato, S., Jaramillo, M. T., Garzón, G., & Mazot, A. (2017). Volatiles and energy released by Puracé volcano. *Bulletin of Volcanology*, 79–84. https://doi.org/10.1007/s00445-017-1168-y

Malinconico, L. L. Jr. (1987). On the variation of SO_2 emission from volcanoes. *Journal of Volcanology and Geothermal Research*, *33*, 231–237. https://doi.org/10.1016/0377-0273(87)90065-5

Marty, B., & Tolstikhin, I. N. (1998). CO_2 fluxes from mid-ocean ridges, arcs and plumes. *Chemical Geology*, *145*, 233–248. https://doi.org/10.1016/S0009-2541(97)00145-9

Monsalve, M. L. (1996). Depósitos piroclásticos asociados a la actividad explosiva del volcán Puracé actual (Colombia), VIII Congreso Colombiano de Geología, Manizales, Tomo III.

Monsalve, M. L., & Pulgarín, B. (1993). Mapa preliminar de Amenaza Volcánica Potencial del Volcán Puracé. Memoria explicativa. *Revista INGEOMINAS*, *2*, 3–27.

Mori, T., & Burton, M. (2006). The SO_2 camera: A simple, fast and cheap method for ground-based imaging of SO_2 in volcanic plumes. *Geophysical Research Letters*, *33*, L24804. https://doi.org/10.1029/2006GL027916

Moussallam, Y., Peters, N., Masias, P., Apaza, F., Barnie, T., Schipper, C. I., et al. (2017). Magmatic gas percolation through the old lava dome of El Misti volcano. *Bulletin of Volcanology*, 46–79. https://doi.org/10.1007/s00445-017-1129-5

Moussallam, Y., Tamburello, G., Peters, N., Apaza, F., Schipper, C. I., Curtis, A., et al. (2017). Volcanic gas emissions and degassing dynamics at Ubinas and Sabancaya volcanoes; implications for the volatile budget of the central volcanic zone. *Journal of Volcanology and Geothermal Research*, *343*, 181–191. https://doi.org/10.1016/j.jvolgeores.2017.06.027

Plank, T. (2014). The chemical composition of subducting sediments. *Treatise on Geochemistry*, *2*(4), 607–629. https://doi.org/10.1016/B978-0-08-095975-7.00319-3

Plank, T., & Langumir, C. H. (1988). The chemical composition of subducting sediment and its consequences for the crust and mantle. *Chemical Geology*, *145*, 325–394. https://doi.org/10.1016/S0009-2541(97)00150-2

Pulgarín, B., Correa, A. M., Cepeda, H. & Ancochea, E. (2001). Aspectos geológicos del complejo volcánico Nevado del Huila (CVNH). Popayán, INGEOMINAS.

Queißer, M., Burton, M., & Kazahayaab, R. (2018). Insights into geological processes with CO_2 remote sensing—A review of technology and applications. *Earth Science Reviews*, *188*, 389–426. https://doi.org/10.1016/j.earscirev.2018.11.016

Sano, Y., Gamo, T., & Williams, S. N. (1997). Secular variations of helium and carbon isotopes at Galeras volcano, Colombia. *Journal of Volcanology and Geothermal Research*, *77*, 255–265. https://doi.org/10.1029/96GL02260

Sano, Y., & Marty, B. (1995). Origin of carbon in fumarolic gas from island arcs. *Chemical Geology*, *119*, 265–274. https://doi.org/10.1016/0009-2541(94)00097-R

Sano, Y., & Williams, S. N. (1996). Fluxes of mantle and subducted carbon along convergent plate boundaries. *Geophysical Research Letters*, *23*(20), 2749–2752. https://doi.org/10.1029/96GL02260

Schipper, C. I., Moussallam, Y., Curtis, A., Peters, N., Bernie, T., Bani, P., et al. (2017). Isotopically ($\delta^{13}C$ and $\delta^{18}O$) heavy volcanic plumes from Central Andean volcanoes: A field study. *Bulletin of Volcanology*, *79*(65). https://doi.org/10.1007/s00445-017-1146-4

Schwandner, F. M., Gunson, M. R., Miller, C. E., Carn, S. A., Eldering, A., Krings, T., et al. (2017). Spaceborne detection of localized carbon dioxide sources. *Science*, *358*(6360). https://doi.org/10.1126/science.aam5782

Shinohara, H. (2005). A new technique to estimate volcanic gas composition: plume measurements with a portable multi-sensor system. *Journal of Volcanology and Geothermal Research*, *143*, 319–333. https://doi.org/10.1016/j.jvolgeores.2004.12.004

Shinohara, H. (2013). Volatile flux from subduction zone volcanoes: Insights from a detailed evaluation of the fluxes from volcanoes in Japan. *Journal of Volcanology and Geothermal Research*, *268*, 46–63. https://doi.org/10.1016/j.jvolgeores.2013.10.007

Shinohara, H., Aiuppa, A., Giudice, G., Gurrieri, S., & Liuzzo, M. (2008). Variation of H_2O/CO_2 and CO_2/SO_2 ratios of volcanic gases discharged by continuous degassing of Mount Etna volcano, Italy. *Journal of Geophysical Research*, *113*, B09203. https://doi.org/10.1029/2007JB005185

Stix, J., Calvache, M. L., & Williams, S. N. (1997). Galeras volcano, Colombia: Interdisciplinary study of a Decade volcano. *Journal of Volcanology and Geothermal Research*, *77*(1-4). https://doi.org/10.1016/S0377-0273(96)00082-0

Stix, J., & de Moor, J. (2018). Understanding and forecasting phreatic eruptions driven by magmatic degassing. *Earth, Planets and Space*, *70*, 10–83. https://doi.org/10.1186/s40623-018-0855-z

Stix, J., Zapata, J. A., Calvache, M. L., Cortes, G. P., Fischer, T. P., Gomez, D., et al. (1993). A model of degassing at Galeras volcano, Colombia, 1988–1993. *Geology*, *21*, 963–967. https://doi.org/10.1130/0091-7613(1993)021<0963:AMODAG>2.3.CO;2

Sturchio, N. C., Williams, S. N., Garcia, N. P., & Londono, A. C. (1988). The hydrothermal system of Nevado del Ruiz volcano, Colombia. *Bulletin of Volcanology*, *50*(6), 399–412. https://doi.org/10.1007/BF01050639

Sturchio, N. C., Williams, S. N., & Sano, Y. (1993). The hydrothermal system of Volcan Puracé, Colombia. *Bulletin of Volcanology*, *55*, 289–296. https://doi.org/10.1007/BF00624356

Syracuse, E. M., & Abers, G. A. (2006). Global compilation of variations in slab depth beneath arc volcanoes and implications. *Geochemistry, Geophysics, Geosystems*, *7*, Q05017. https://doi.org/10.1029/2005GC001045

Tamburello, G. (2015). Ratiocalc: Software for processing data from multicomponent volcanic gas analyzers. *Computational Geosciences*, *82*, 63–67. https://doi.org/10.1016/j.cageo.2015.05.004

Tamburello, G., Agusto, M., Caselli, A., Tassi, F., Vaselli, O., Calabrese, S., et al. (2015). Intense magmatic degassing through the lake of Copahue volcano, 2013–2014. *Journal of Geophysical Research: Solid Earth*, *120*, 6071–6084. https://doi.org/10.1002/2015JB012160

Tamburello, G., Aiuppa, A., Kantzas, E. P., McGonigle, A. J. S., & Ripepe, M. (2012). Passive vs. active degassing modes at an open-vent volcano (Stromboli, Italy). *Earth and Planetary Sciences Letters*, *359–360*, 106–116. https://doi.org/10.1016/j.epsl.2012.09.050

Tamburello, G., Hansteen, T., Bredemeyer, S., Aiuppa, A., & Tassi, F. (2014). Gas emissions from five volcanoes in northern Chile and implications for the volatiles budget of the Central Volcanic Zone. *Geophysical Research Letters*, *41*, 4961–4969. https://doi.org/10.1002/2014GL060653

Tamburello, G., Kantzas, E. P., McGonigle, A. J. S., & Aiuppa, A. (2011). Vulcamera: A program for measuring volcanic SO_2 using UV cameras. *Annals of Geophysics*, *54*(2), 219–221. https://doi.org/10.4401/ag-5181

Tamburello, G., Kantzas, E. P., McGonigle, A. J. S., Aiuppa, A., & Gaetano, G. (2011). UV camera measurements of fumarole field degassing (La Fossa crater, Vulcano Island). *Journal of Volcanology and Geothermal Research*, *199*(1-2), 47–52. https://doi.org/10.1016/j.jvolgeores.2010.10.004

Tamburello, G., Pondrelli, S., Chiodini, G., & Rouwet, D. (2018). Global-scale control of extensional tectonics on CO_2 Earth degassing. *Nature Communications*, *9*. https://doi.org/10.1038/s41467-018-07087-z

Thouret, J. C., Cantagrel, J. M., Salinas, R., & Murcia, S. (1990). Quaternary eruptive history of Nevado del Ruiz (Colombia). *Journal of Volcanology and Geothermal Research*, *41*, 225–251. https://doi.org/10.1016/0377-0273(90)90090-3

Thouret, J. C., Vatin-Perignon, N., Cantagrel, J. M., Salinas, R., & Murcia, A. (1985). Le Nevado del Ruiz (Cordillere Central des Andes de Colombie): Stratigraphie, structures et dynamisme d'un appareil volcanique andesitique, compose et polygenique. *Revue de géologie dynamique et de géographie physique*, *26*, 257–271.

Voight, B. (1990). The 1985 Nevado del Ruiz volcano catastrophe: Anatomy and retrospection. *Journal of Volcanology and Geothermal Research*, *44*, 349–386. https://doi.org/10.1016/0377-0273(90)90027-D

Voight, B., Calvache, M. L., Hall, M. L., & Monsalve, M. L. (2016). Nevado del Ruiz volcano, Colombia 1985. In P. T. Bobrowsky (Ed.), *Encyclopedia of natural hazards. Encyclopedia of Earth Sciences Series* (pp. 732–738). Dordrecht: Springer. https://doi.org/10.1007/978-1-4020-4399-4_253

von Huene, R., & Scholl, D. W. (1991). Observations at convergent margins concerning sediment subduction, subduction erosion, and the growth of continental crust. *Reviews of Geophysics*, *29*, 279–316. https://doi.org/10.1029/91RG00969

Wallace, P. J., Plank, T., Edmonds, M., & Hauri, E. H. (2015). Volatiles in magmas. In H. Sigurdsson, B. Houghton, S. McNutt, H. Rymer, & J. Stix (Eds.), *The encyclopedia of volcanoes* (2nd ed., pp. 163–183). San Diego, CL: Elsevier Inc., Academic Press.

Zapata, J. A., Calvache, M. L., Cortés, G. P., Fischer, T. P., Garzon, G., Gómez, D., et al. (1997). SO_2 fluxes from Galeras volcano, Colombia, 1989–1995: Progressive degassing and conduit obstruction of a Decade Volcano. *Journal of Volcanology and Geothermal Research*, *77*, 195–208. https://doi.org/10.1016/S0377-0273(96)00094-7